Reviews in Computational Chemistry Vol 22, pp 229-294 (2006)

The Simulation of Ionic Charge Transport in Biological Ion Channels: an Introduction to Numerical Methods

Marco Saraniti*, Shela Aboud†, and Robert Eisenberg†

January 14, 2005

*Electrical and Computer Engineering Department, Illinois Institute of Technology, Chicago, IL

†Department of Molecular Biophysiscs and Physiology, Rush University, Chicago, IL

1 Introduction

Ion channels are proteins embedded in the lipid membrane of biological cells. They interact in a complex way with their environment and are responsible for finely regulating the flux of ionic charge across the membrane. For instance, the generation and transmission of potentials in nerves and muscles, as well as the hormone release from endocrine cells, are believed to be mechanisms governed by the transport of ionic charge through these protein "gates" [1].

Since the demonstration in 1976 [2] of a reliable experimental methodology for the detection of currents flowing through individual ion channels, several refinements of the experimental setup have been successfully applied to a variety of membrane and cell configurations, both *in vivo* and *in vitro* [3]. The extraordinary progress of those experimental techniques triggered an increasing theoretical effort aimed at the understanding of the role of ion channels in the physiology of complex biological systems, and, more generally, their influence on the electrical equilibrium between the cells and their environment. Besides the purely theoretical aspect, important pharmacological advances have arisen from improved knowledge of ion channels [4]. Furthermore, from an engineering viewpoint, ion channels are being envisioned as a key component in a new generation of biosensors that integrate the selectivity and extreme sensitivity of ion channels with the processing capabilities of modern microelectronics [5, 6, 7].

The appeal of the many possible applications of ion channels is only one part of the complete story. The interest of the computer modeling community has also been triggered by several concomitant events: *1)* the availability of reliable protein structural data, *2)* the capability of producing mutants by reprogramming the genetic sequence of bacteria, *3)* the availability of reproducible experimental data on the electrophysiology of individual channels, and *4)* the availability of adequate computational machinery (hardware *and* software) for the realistic modeling and simulation of ion channels in their environment. All these contributions occurred more or less simultaneously during the last decade, and produced a rather unusual synergy among experimentalists, theoreticians,

and computational scientists who combined their efforts in order to relate the structure of ion channels to their function.

A peculiar aspect of the research on ion channels is that it frequently involves researchers working in traditionally different disciplines. The solid-state electronics community, for example, is well aware of the fact that traditional scaling – *i.e.*, the reduction of the feature-size of transistors needed to increase the performance of integrated circuits [8] – will soon be inadequate to satisfy the requirements of emerging technologies [9]. A natural solution is to increase the complexity rather than the speed of the basic components, and much can be learned from ion channels, which are extremely specialized and miniaturized low power devices. Transistors are definitely faster than ion channels, but the advantage due to their operational speed is compensated by the complexity of the operations performed by ion channels. It appears clear that the full understanding of ion channel properties will allow for either the modification of their design for novel applications, or for manufacturing analogous structures capable of emulating their functionality.

This chapter is intended to be an introduction to the numerical techniques used for the simulation of charge transport through ion channels. The complexity and the size of the systems to be simulated will be stressed throughout the entire chapter, as well as the potential for the practical applications of ion channels in several fields. We firmly believe that the computer simulation of ion channels is not just a "large scale" problem that will be progressively solved as computer performance naturally evolves. High performance computing is only one component of the solution, and much work is needed for devising and integrating adequate physical models and algorithmic approaches. Therefore, ion channel simulation is a good example of the assertion that "computers do not solve problems, people do" [10].

In addition to the introduction, this chapter consists of four main sections and some concluding remarks. First, a description of the computational methods used to model the electrostatic framework of ion channels is given, including a discussion of the boundary conditions traditionally used. A rather detailed

description of efficient algorithms for the solution of Poisson's equation in real space is supplied for representing the long-range electrostatics of ion channel systems. This approach has been identified as a possible improvement of the force-field models used in particle-based simulation (molecular and Brownian dynamics) [11, 12], but its popularity is low because it has been limited to simple test problems. The two following sections are devoted to the various models of ionic charge transport through the channels. In particular, a classification of continuum and particle-based methods is provided, and a discussion of their modeling capabilities is presented. The need for a hierarchy of numerical approaches needed to model the behavior of the systems of interest at different time and space scales is discussed in the penultimate section. The last section is devoted to problems that are still open, and to the future direction of research on the numerical simulation of biological ion channels. For reasons of space, this chapter focuses mainly on the numerical methods used to directly model charge transport in biological ion channels. However, it should be noted that a great deal of information on these systems and their properties is obtained with other techniques such as quantum chemistry (or structural *ab initio*) methods and by stochastic sampling approaches for the analysis of trajectories in the phase-space (Monte Carlo methods).

The remaining part of the introduction will be devoted to the description of the simulative environment required to model the operation of ion channels.

1.1 System Components

Ion channels interact strongly with their environment. From a microscopic viewpoint, these proteins cross the lipid bilayer that forms the cell membrane, and are exposed to the electrochemically different environments found inside and outside the cell. They are designed to react in a highly specialized way to specific stimuli – mechanical, chemical, or electrical – and to express their function by regulating the ionic flux across the cell membrane. For this reason, any simulative approach meant to model ion channels must account *in some*

way for the combined behavior of the protein channel, the membrane, and the aqueous solution containing the ionic species of interest. Additionally, a way to represent a specific stimulus must be devised, in order to model the transient behavior of the channels as a function of the "external" perturbation.

1.1.1 The Protein

Because of the highly specialized functions they perform, ion channels are classified into different families. These families are based upon the ions those channels selectively allow to flow into and out of the cell. This functional classification [1] has been adopted as a result of the early electrophysiologic experiments on ion channels, and its success is due to the strict relation between the structure of the channels and their function. It should be noted that several channels that allow the diffusive flow of non-ionized substances across the membrane exist, an example of which are the mechano-sensitive channels regulating the bacterial cytoplasmic pressure by responding to membrane tension [13]. Most of the basic models discussed in this chapter apply to these diffusive channels as well.

Most of the membrane proteins contain α-helices and β-sheets connected in structures of varying complexity. Within a specific structure, some helices cross the membrane from one side to the other, while other segments of the protein are confined in a more limited region. The amino-acid sequences are structured in such a way that one or more pores are formed inside the protein, that are large enough to allow for ionic flow. The protein structure is flexible and, in many cases, the functionality of ion channels is achieved by structural changes occurring in specific locations of the amino acid sequence.

From the functional viewpoint, we will discuss mainly the operations of ion channels in relation to the following three properties: *permeation*, which is the property of allowing ions to cross the strong dielectric barrier due to the cell membrane; *selectivity*, which is the capability of discriminating between the ionic species flowing through the channel structure; and *gating*, which is the capability of modulating the flux through the channel in response to an exter-

nal stimulus. It is important to note that gating occurs on a time scale several order of magnitude longer than the typical transit time of one ion though the channel pore. This is a critical aspect of these systems that must be accounted for in the simulation: the crucial physics occurs on distances measured in a few angstroms and starts on a femtosecond time scale, while the resulting physiological functionality is expressed in milliseconds and on distances measured in microns. The ability to relate the ultrafast microscopic processes occurring in channel proteins to their slow physiological expression is *the* challenge of ion channels simulation.

The structural features of some channels will be presented briefly in the remaining part of this introduction. This discussion is not meant to offer a classification of ion channels, but rather some key features of notable structures that are used as examples in this chapter. The three channels we now describe are: Gramicidin A, potassium channels and finally porins.

Gramicidin A Gramicidin A (gA) is a small 15-residue antibiotic peptide formed as a dimer in a head-to-head (HH) or a double-helical (DH) conformation [14]. Because of its simplicity and reduced dimensions, the gA structure has been studied extensively and simulated as a model for ion channels [15, 16, 17, 18, 19], and has emerged as a benchmark for simulation approaches [20, 21, 22, 23, 24]. The structure exposes its hydrophobic sidechains to the lipid membrane that embeds the protein. The molecular structure of gA has been known for three decades [25], and has been recently resolved with NMR spectroscopy [26, 27]. The relation of the structure seen spectroscopically to that in membranes which conducts ions is being investigated [28]. Figure 1 shows the gA backbone structure perpendicular to the pore and a top view along the backbone structure showing the hydrophobic sidechains for the (a) DH [29] and (b) HH [30] conformations. The interaction of the protein with the lipid bilayer (hydrophobic matching) has been modeled quantitatively [31, 32] and measured experimentally [33], as has its properties of water transport [14, 34]. Concerning gating, characteristically fast (sub-millisecond) closure events, called

flickers, have been attributed to either conformational changes (lateral shifts of the monomers [35]) triggered by the breaking of the hydrogen bonds joining the dimer in the HH configuration, or by undulations of the bilayer that modify the conductive state of the protein [36]. Novel experimental techniques, such as patch-clamp fluorescence microscopy [37], are being devised for detailed observation of the conformational changes of this simple structure. From a charge transport viewpoint, gA selects monovalent cations and its conductivity depends on both the membrane conformation and the ionic concentration surrounding it [38].

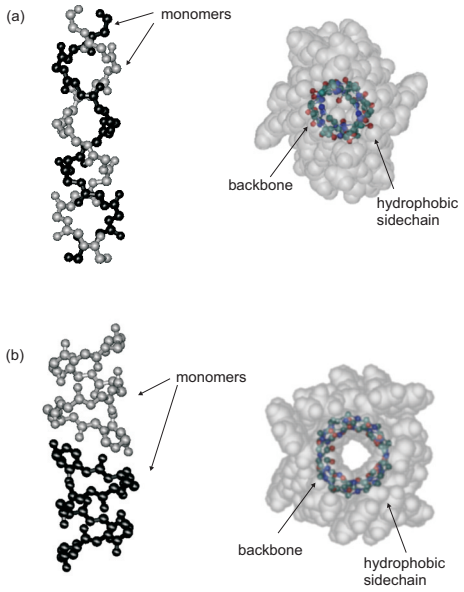

Figure 1: Atomic structure of a (a) double-helical (1mic.pdb [29])and (b) head-to-head (1mag.pdb [30]) conformation of Gramicidin A. The pictures to the left show the backbone representation perpendicular to the pore. The pictures to the right show a view parallel to the channel that includes the hydrophobic sidechains. The pictures were generated with VMD [39].

Potassium channels Potassium channel, or K-channels are present in nearly all cells [1], and play a key role in stabilizing the membrane potential in excitable

cells. They are therefore crucial for the electrical functionality of the nervous system. They are characterized by an extreme selectivity (their permeability for K^+ is thousands of times larger than that of the smaller Na^+ ions), and by a high diffusivity (comparable to bulk water). The molecular structure of several K-channels has been disclosed by means of X-ray spectroscopy. In particular, a 3.2 Å resolution mapping of the pH-dependent bacterial KcsA channel was performed by Doyle *et al.* [40], and a higher resolution (2.0 Å) structure has been subsequently disclosed by the same group [41]. The structure of the ligand-gated MthK channel, which opens in response to intracellular Ca^{2+} [42] has also been determined, and the structure of the voltage-gated [43] KvAP channel has been published recently [44]. Together with accurate structural data, several hypotheses about the functionality of these ion channels have been formulated.

The three K-channels listed above are tetrameric assemblies with sub-units sharing the same signature amino acid sequence TXGYGD of the selectivity filter. Also common is the topology of the ionic permeation channel, composed of two transmembrane helices (inner and outer helix) per sub-unit. The two transmembrane helices are joined by a pore sequence constructed with a shorter pore helix plus the selectivity filter segment.

The KcsA channel is characterized by this simple two transmembrane architecture (see [40], and the left side of Fig. 2), and its activation has been attributed to pH-dependent translations and rotations of the two transmembrane helices [45]. Because of its relative simplicity, KcsA has been simulated extensively with a variety of approaches, and, like gA, it too can be considered a benchmark system for simulation codes [38].

The MthK channel has an additional large gating ring below the membrane-spanning pore (right side of Fig. 2, the gating ring is not included). The gating ring is responsible for converting the free energy of intracellular Ca^{2+} into mechanical work that pulls apart the helices of the transmembrane pore and opens it to allow potassium permeation [42]. Finally, the sequence of the voltage-dependent KvAP channel shows six transmembrane helices: the same two hydrophobic segments of KcsA and MthK (segments S5 and S6) and four

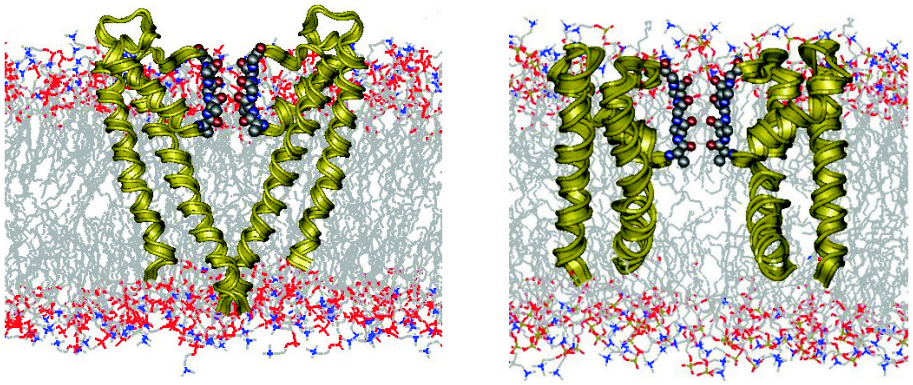

Figure 2: Two sub-units of the KcsA (left) and MthK (right) potassium channels embedded in an explicit POPC lipid bilayer. The atoms lining the selectivity filter are represented as spheres to show the individual "cages" which represent the binding sites of K^+ ions. The KcsA and MthK structures are obtained from the protein database codes 1bl8.pdb [40] and 1lnq.pdb [42], respectively

additional helices (S1-S4) that constitute the voltage-activated gate. A section of S3 (S3b) and S4 define a mobile "voltage-sensor paddle" [44]. Recent experiments [46] suggested that, due to the presence of charged amino acids in S4, the channel undergoes a dramatic conformational change in the presence of an adequate transmembrane voltage: the "paddle" rotates more or less rigidly and crosses most of the lipid membrane pulling open the pore made by the helices S5 and S6. This interpretation of the gating mechanism of MthK is currently under intense investigation (see for example [47]).

The permeation path of K-channels shows a very irregular (but highly functional) profile [38]: a hydrated ion moves (outward) initially through the intracellular gate made by the tips of the inner helices, enters a large central cavity (that probably favors monovalent cations over intracellular polyvalent cations [48]) filled with tens of water molecules, and then crosses the extremely narrow (angstrom size) selectivity filter where its solvation is at least partially due to carbonyl oxygen atoms rather than water [41]. A potassium ion therefore changes its hydration configuration during the journey, and travels an electro-

statically irregular pathway to exit the cell. K-channels are engineered in such a way that this process is extremely fast and highly K-selective.

Porins Porins are the first channels for which an atomic crystal structure was available [1]. These proteins function as ion channels with high conductivity and relatively low selectivity [38]. Because of the availability of experimental data [49], porins have been used extensively to build and test simulation methods for ion channels. Many mutants of the bacterial trimer OmpF have been synthesized and modeled [50]. The permeation process has been simulated with different molecular dynamics approaches [51, 52]. OmpF is a relatively large polypeptide made of three monomers composed of 340 amino acid each. The monomer is a hollow β-barrel structure formed by 16 antiparallel β-strands. The structure has eight loops (L1-L8) that form the water-filled pore. Loop L3 folds inside the barrel and generates a structural constriction that reduces the lumen of the pore to a diameter of approximately 6 Å. A top view of the three monomers of OmpF (protein database code 2omf.pdb [53]) is shown in Fig. 3 (right), where the L3 loops are represented by the large shaded cylinders. The OmpF crystal structure embedded in an explicit lipid membrane is also shown on the left side of Fig. 3. The charge distribution in the proximity of the constriction and all over the length of the pore, plays a crucial role in the permeation properties of OmpF. Furthermore, the close proximity of negative and positive charges within the constriction zone generates an intense electric field that interacts with ions and determines the channel conductivity. The ionization state of the residues in the pore changes with the pH of the solution, suggesting that OmpF may function as a pH-gated channel in some conditions. The role of the conformational changes due to molecular flexibility (particularly for the L3 loop) is still an open question for the understanding of the functionality of OmpF.

The electrical properties of OmpF have been measured for long times, both with patch-clamp techniques and on planar lipid membranes [49]. A high-resolution electrostatic mapping of the trimer was obtained with atomic probe

microscopy [54], while a systematic electrostatic modeling of the pore lumen has been performed by two groups [51, 50] who did not limit their study to the wild protein, but comparatively analyzed several mutants. The electrostatic landscape of OmpF is a typical example of how the balance between strong interactions finely tunes the properties of a channel. Ionic trajectories have been simulated both with Brownian and molecular dynamics simulation codes [52], and the role of ion-ion interaction within the pore has been stressed as being important.

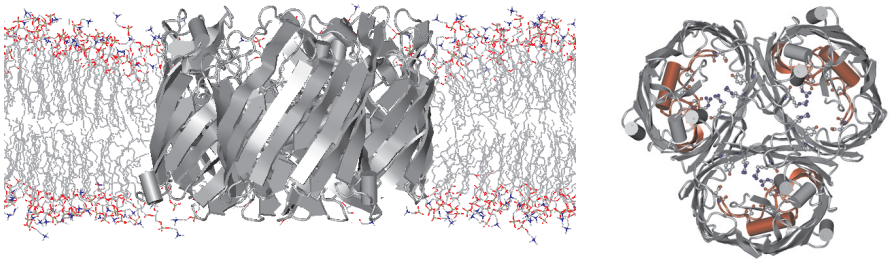

Figure 3: The OmpF porin channel (left) embedded in an explicit POPC membrane, and (right) the corresponding top view of the OmpF. The L3 loop in the constriction zone of the three monomers is represented by the large shaded cylinder. The structure has been obtained from the protein database (2ompf.pdb) [53] and the plot has been rendered with VMD [39].

1.1.2 The Membrane

The cell membrane is made of amphipathic molecules consisting of one polar, hydrophilic head and one (or two) nonpolar, hydrophobic tails [55]. In an aqueous environment the lipid molecules spontaneously aggregate into conformations that minimize the interaction between water molecules and the hydrophobic tails of the lipids. One configuration that is energetically favorable is that where the lipid bilayer [56], composed of two parallel sheets of lipid molecules, is oriented in such a way that the molecular heads are in contact with the aqueous solution and the tails are inside the membrane thickness. Under conditions of normal

cell function, the lipid is an extremely stable two-dimensional structure that rapidly reassembles itself if disturbed or broken.

The three main classes of lipids present in cell membranes are phospholipids, glycolipids and cholesterol [57]. Phospholipids are the most abundant of the biological membrane lipids and are assembled from fatty acids, alcohol and phosphate. The hydrophilic head is composed of an alcohol (such as choline) joined through a phosphate to either glycerol or sphingosine. Fatty acid hydrocarbon chains are attached to the lipid molecule through the glycerol or sphingosine and constitute the hydrophobic tails. The phospholipids based on glycerol are called phosphoglycerides while those based on sphingosine are called sphingolipids. The phosphatidylcholine (POPC) molecule, shown in Fig. 4 is the most common phosphoglyceride in biological cells [57], and is characterized by a choline molecule attached to the phosphate at the hydrophilic head. Additionally, one of the hydrocarbon tails is fully saturated while the other contains several unsaturated bonds, creating the tail kinks shown in Fig. 4. The fluidity, or lateral diffusion of lipid molecules within the bilayer, depends on the length and saturation of the hydrocarbon tails. A cross section of a lipid bilayer formed with POPC molecules is shown in Fig. 5. Long hydrocarbon chains increase the "drag" on a lipid while unsaturated bonds improve the lipid mobility due to the reduction of the overall packing density. The phospholipid sphingomyelin is distinguished from POPC by a long hydrocarbon chain of sphingosine which substitutes for one of the fatty acids in the hydrophobic tails.

The second class of lipids are glycolipids. They are structurally similar to sphingomyelin except they contain sugar residues, such as glucose or galactose, instead of the phosphate-alcohol group in the hydrophilic head. The sugar residues in glycolipids are always oriented on the extracellular side of the membrane and form part of the carbohydrate coating that surrounds most animal cells.

Cholesterol is a steroid that has a different structure than either phospholipids or glycolipids. The body is constructed primarily of four hydrocarbon rings. The polar head is formed by a hydroxyl group attached at one end while

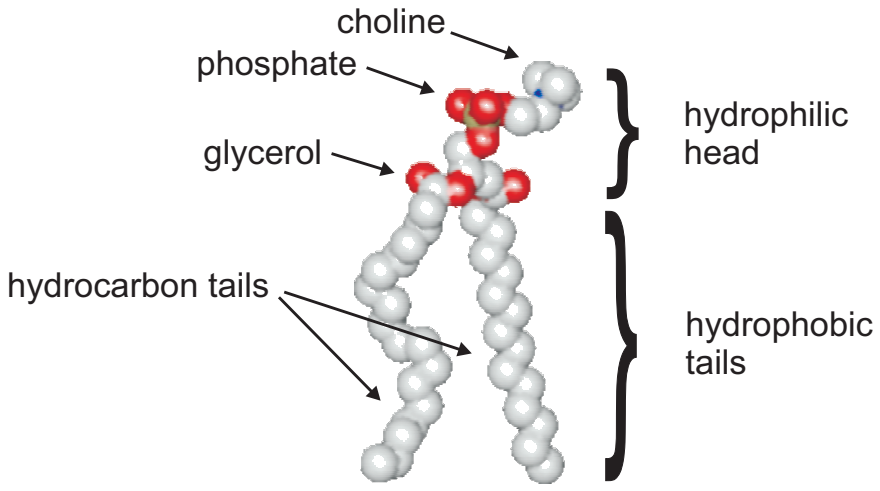

Figure 4: The head group of the lipid molecule phosphatidylcholin is composed by a choline, a phosphate and a glycerol, while the hydrophobic tails are formed from two fatty acid chains. The atomic coordinates of the lipid molecule are from the work of Tieleman *et al.* [58], and the plot is rendered with VMD [39].

a long saturated hydorphobic hydrocarbon tail is attached to the other end of the ring system. The steroid rings form a rigid planar structure that reduces the fluidity of the plasma membrane. In animal cells, cholesterol molecules are located between the phospholipids, filling the spaces from the kinked unsaturated bonds of the hydrocarbon tails thus making the lipid more rigid.

The precise composition of the lipid membrane in biological cells is inherently complex, and varies depending on both the species and type of cell. In addition, the local distribution of the lipid molecules within a single bilayer can be highly disordered, and, the two corresponding monolayers are generally asymmetric [55]. The inclusion of transmembrane structures, such as ion channel proteins and polymers, further complicates the picture. The extremely heterogeneous nature of the bilayer combined with the flexibility and polarizability of the lipid molecules makes the study of membranes in real biological systems a formidable task, both from the experimental and the computational viewpoint.

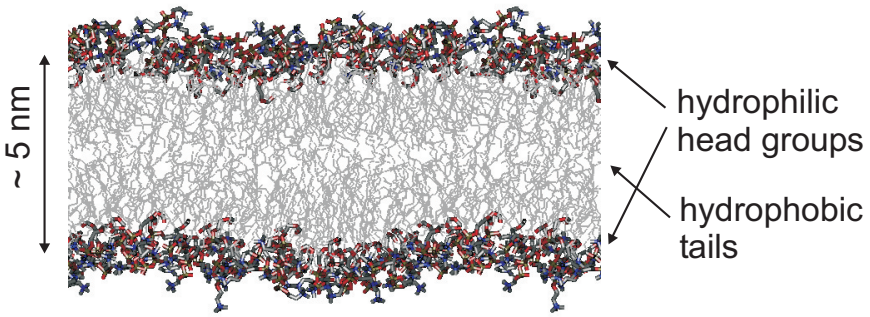

Figure 5: Cross section of a membrane composed of phosphatydylcholine molecules. The graphic rendering has been obtained with VMD [39].

Because of the fluctuations of the flexible biological membranes, the structural characterization of lipid bilayers is an arduous task when atomic details are sought [59]. Indeed, structural information about the membrane thicknesses, such as the hydrophobic thickness and head group separation, as well as the lipid density, are very difficult to quantify. This results in a large uncertainty in the experimentally determined structural parameters of lipid bilayers found in the literature. For example, values of the average area per phospholipid molecule measured in a single lipid system can vary by nearly 30 Å^2 [59].

The simulation of lipid bilayers provides a method for probing microscopic details of the lipid system, and relates those details to the macroscopic behavior observed experimentally [56, 60]. The molecular dynamics approach is the most popular choice for membrane simulation, because it provides information about the spatial and temporal evolution of both single species phospholipid membranes [61, 62], and multi-lipid systems [63, 64, 65]. For example, molecular dynamics allowed for the characterization of phospholipid bilayers in terms of their interaction with water, and revealed that the orientation of the water molecules compensated for the fluctuations in the lipid head group, resulting in an almost constant membrane dipole potential [61, 66].

Although molecular dynamics is arguably the most accurate simulation technique, the characteristic relaxation times of the lipid system are generally orders of magnitude larger than the time that is needed to obtain statistically significant results [67, 62]. Also, the space scale over which the lipids self-organize can exceed the size of the computational domain that can be realistically simulated with extant molecular dynamics techniques.

1.1.3 The Aqueous Environment

Aqueous solutions under biologically relevant conditions are composed primarily of water molecules; water therefore plays a primary role in many chemical and physical processes [68]. Water is a highly polar molecule due to its bent configuration. A spatial separation exists between the internal positive and negative charges in the electrically neutral molecule, giving rise to a strong, permanent electric polarization field [69]. Furthermore, the separation between internal charges makes it possible for the oxygen atom of one water molecule to bond electrostatically to the hydrogen atoms in neighboring molecules. This hydrogen bonding facilitates the formation of relatively large domains of water molecules into lattice-type structures [69] analogous to crystalline ice. This cluster configuration of liquid water is not static and domains are continually formed and disassociated.

Ions in aqueous solution alter the structure of water in such a way that the water molecules will orient themselves around the charged ions with the appropriate polar side of the water pointing toward the ion, and creating one or more hydration shells. The water in the hydration shell now behaves differently than the bulk water in the sense that its dynamics is correlated with the ionic motion.

Aqueous solutions confined in regions of molecular dimensions, such as the narrow pores of ion channels, exhibit different properties than bulk ionic solutions, and one way to characterize the microscopic properties of ion channels is to identify these differences [38]. Confinement in small regions restricts the

translational and rotational motion of the water molecules, and creates a greater degree of order. Simulations revealed a consequently strong decrease of the diffusion coefficient in small water-filled cavities. In addition to the effects of the physical confinement, a significant electrostatic interaction is also present between the water molecules and the cavity walls. In the case of porin channels, for example, the internal transverse electric field is so high that the cavity region is no longer a linear dielectric medium. [38]. Polar groups in the pore lining interact with the water molecules in the hydration shell of ions as they traverse the pore, and this interaction may play a direct role in the selectivity properties of protein channels [38, 70].

Although not rigorously correct, the approximation of water as a structureless homogeneous continuum dielectric medium is used by many simulative methodologies. Both Brownian dynamics (see the section entitled Implicit Solvation: Brownian Dynamics) and electrodiffusive approaches (see the section on Flux-Based Simulation) include the water in the electrostatic picture as a continuous dielectric background with polarizability appropriately tuned inside the channel pore. These "implicit water" models are able to reproduce activity coefficients for a variety of bulk systems [71, 72, 73] as well as the conductivity behavior of ions through channels [22]. Obviously, care must be taken when applying these techniques to model ion transport in channels where individual water molecules play a crucial role [23], such as within the extremely narrow selectivity filter of potassium channels.

1.1.4 Representing the Full System

The definition of the system to be simulated, as well as the choice of the details in its representation, are crucial for the simulation of ionic transport in protein channel systems. Several components, including the channel itself, can be represented *implicitly*, that is through some macroscopic properties representative of their effects on the simulative landscape, or *explicitly*, that is with a microscopic, atomic-scale, resolution that is governed by fundamental laws.

The model used for the computational representation depends on the specific questions to be addressed [74].

For instance, an implicit membrane model greatly reduces the computational burden, and is appropriate in many cases because the lipid-protein interaction is often only important for protein stability and insertion [75]. In addition, the time scale of the charge transport process across the membrane is usually much longer than the time scale of the lipid fluctuations, so the motion of the charge is influenced primarily by the membrane through its dielectric rather than dynamics properties. Within the implicit bilayer representation, the membrane is treated as an impermeable slab of either a homogeneous dielectric material, or as a slab with a low dielectric constant in the region of the nonpolar tails and a higher effective dielectric constant in the region where the charged head groups of the lipids reside [76, 53].

When the interaction between membrane and protein channels becomes significant at the atomic level, an explicit representation of the molecules forming the lipid bilayer and protein channels must be built and modeled in such a way that the mechanical, chemical, and electrostatic properties of the system are modeled with appropriate detail. Two basics techniques generally have been used to build a channel/membrane system with atomic resolution. One approach consists of seeding the bilayer by placing individual pre-equilibrated lipid molecules in appropriately chosen locations around the protein structure [77, 52]; the membrane is then grown by attaching other lipid molecules to those previously connected to the channel. The second technique consists of generating a protein-shaped cavity in the center of a previously equilibrated lipid bilayer and inserting the transmembrane protein channel into the cavity.

In both approaches a series of equilibration steps based on energy minimization [78] is used to obtain the final configuration of the lipid/protein system. In the latter case, the process does not affect the initial lipid configuration significantly outside the cavity region, and the final configuration of the lipid/protein system will be very close to the equilibrium structure, thus making it an attractive computational choice.

Several methods to generate a cavity in a lipid bilayer exist. The simplest approach is to remove a cylindrical section of lipid molecules [79] and insert the protein channel into that void. Because lipids are removed in molecular units, the boundary region between the lipid tails and the cylindrical hole tends to be rough. Therefore, many equilibration steps may be required after the protein is inserted, resulting in an unacceptably slow convergence, or in a possibly wrong, unstable, or metastable configuration. An improved approach consists of using a weak cylindrical repulsive force [80] to slowly create the cavity, rather than removing the lipids located inside the region of the cavity. This approach has the benefit of creating a smoother surface at the boundary of the lipid/protein interface. However, the techniques based on approximating the protein molecular surface with a cylinder can result in a difficult equilibration process when non-cylindrical proteins are inserted into the cavity. To address this problem, an arbitrary shaped cavity is obtained by superimposing an atom-size three dimensional grid over the system built by imposing the protein on the lipid patch [79]. All lipid molecules that intersect grid cells containing protein atoms are then removed. Energy minimization steps are then used to further refine the position of the lipids' atoms. Alternatively, a smooth membrane/protein interface with arbitrary geometry can be obtained by applying a weak radial force to create the cavity. In this case, the van der Waals surface [81] of the protein is generated and superimposed on a preequilibrated lipid patch [82]. The lipid atoms inside the van der Waals surface experience an outward radial force, that pushes them out of the cavity. This process is repeated until the hole exactly matches the outer van der Waals surface of the protein.

1.2 Time and Space Scale

After choosing an adequate model for each different component of the system and integrating them into a final atomistic model that will be simulated, an important issue is the selection of a discretization scheme to implement the computer representation of the ion channel and its environment. Within the

framework of a computer experiment [83], the adjective *realistic* is strictly related to the phenomena one wants to study, and to the resolution required to reproduce those phenomena. The basic idea for modeling many-body systems is to build a set of rules that apply to each component and let the system evolve dynamically. Ensemble and time averages are then computed to obtain observables that are compared with experiment to validate the model. A characteristic of ion channel systems is that the measurable quantities of direct biological interest evolve in times up to 12 orders of magnitude larger than the smallest atomic or molecular relaxation times (milliseconds versus femtoseconds). In comparison, solid state many-body systems collectively relax in a faster fashion, and the difference between the microscopic (simulated) and macroscopic (measured) dynamics is four or five order of magnitudes. Extremely slow events, such as charge carrier recombination in semiconductor crystals, also exist in solid state systems, but they can be accounted for in a relatively easy way.

The atomistic representation of a fully hydrated membrane/channel system requires an extremely large number of atoms distributed irregularly on a large computational domain. As an example, consider a K-channel embedded in a POPC membrane as depicted in Fig. 2. The diameter of the selectivity filter in the protein is a few angstroms, and the ionic transit inside the channel occurs in about a microsecond. The selectivity itself is a process that depends on the electrodynamic reaction of the atoms forming the selectivity filter to the electrical and polarization fields due to ions and water inside the filter itself. Given the extremely small distances between the charged components of the system, one expects an extremely rapid relaxation (about ten femtoseconds) that changes the dielectric environment inside the filter. So one needs to simulate the system for a few nanoseconds with a resolution of a few femtoseconds in order to observe the transit of one individual ion across the entire structure.

Analogously, the channel functionality depends on structural characteristics that extend over a large distance. The interaction of the channel with the membrane is sometimes crucial, both from the structural and electrostatic viewpoint. Furthermore, the structural changes involved in gating are the result of, or are

involved directly in, the interaction of the outer protein segments with the membrane. All these facts necessitate the representation of a relatively large system that has to be resolved with angstrom-size accuracy.

Because of the problems related to simulating a large system for a long time with an extremely high resolution, a crucial issue is related to the number of atoms or groups of atoms needed to represent such a system. Indeed, if a brute-force atom-based method is used, the number of individual particles to be simulated is extremely large. In principle, the atomistic representation of a whole protein and of a sufficiently large patch of membrane requires the modeling of at least tens of thousands of particles subjected to a constrained non-local dynamics. Solvation effects must also be accounted for to correctly model both the ion dynamics and the structural properties of the whole system. Biological solutions are typically 0.2 Molar salt but approximatively 55 Molar water. This implies the need for a water model and, consequently, the dramatic increase of the size of the system being simulated.

1.3 Experiments

As previously mentioned, a decisive contribution to the understanding of ion channels has been supplied from experiments. The electrical activity of individual channels is measured both *in vivo* and *in vitro* under various conditions [3]. While the description of experimental setup for channels recording is beyond the scope of this chapter, an important aspect concerning the relevance of the experiments done on channels and their connection with computer modeling should be stressed. Current experiments are not limited to a "simple" observation and characterization of natural channels, but allow for the study of man-made, designed proteins. This capability of building mutant channels by substituting amino acids into the sequence of the natural (or wild) proteins is important for the functional characterization of ion channels, and for the realization of novel macromolecules with specific tunable properties. The need for a strict integration of computational structural chemistry with protein engineering is clear, as

well as the need for efficient and reliable computational tools that can direct the experimental work and, at the same time, be validated by it.

2 Electrostatics

The channel-membrane-solution system is characterized by an inhomogeneous charge distribution that conditionally allows mobile ions to cross the strong dielectric barrier [84] imposed by the membrane. Therefore, an accurate representation of the electrostatic forces acting on each component is needed understand the influence of the system's structural properties on its function.

The force fields used by scientists for simulations have been developed with distinct traditions, each appropriate for its own use. In computational chemistry, interest has been in bulk properties of solutions and proteins, in the thermodynamic limit in which boundary conditions do not appear explicitly and where equilibrium (*i.e.*, zero flux of all species) is present. The thermodynamic limit of computational chemistry implies a spatial uniformity of bulk properties that can be analyzed with periodic boundary conditions [85] if the period is longer than the spatial inhomogeneities of the bulk solution [86].

Contrarily, in computational electronics, the interest has focused on electron devices, which exchange charge with their environment through geometrically and electrically complex boundaries and where internal dielectric discontinuities exist. Simulations are usually performed by varying the applied bias in order to reproduce transient nonequilibrium conditions and to obtain a record of the response of the simulated devices.

Given the substantial differences between the systems being simulated, the force-fields traditionally used by researchers in computational electronics and in chemistry are necessarily different. In particular, short-range coulombic interactions are either neglected in electron device simulations, or they are treated with a stochastic approach [87] rather than deterministically. The same considerations apply for finite size effects.

In the highly inhomogeneous charge distribution of ion channel systems

makes them closer to electron devices than to bulk homogeneous systems. This analogy encouraged us to develop the discussion in this tutorial from the viewpoints of both computational electronics and chemistry. The idea here is not to compare the two traditions of computational science, but instead to approach the modeling problem with an interdisciplinary attitude.

Given the complex dynamic properties of the ion channel system, many studies have been performed to examine whether or not any reduced representation could be used to account for some key properties. These attempts have been performed both by theoreticians *and* experimentalists by simulating and measuring properties of simplified systems. From the modeling viewpoint, the evolution of the work of Jordan [88, 89, 90, 91], among others, shows how experimentally obtained structural information has been included into an increasingly complex electrostatic picture as that data became available. Also, the importance of the charge distribution within protein channels is highlighted by the recent work of Varma and Jakobsson [50], who conducted a systematic study of the ionization states within the lumen of a large porin in order to assess the charge assignment protocols used in the simulation code. Due to the small dimension of ion channels, charges of ions and protein residues are concentrated in small areas. The effects of this "crowded charge" configuration generate extremely localized electric fields that have a significant effect on the polarization state of the system, and perhaps on the molecular structure of the ion channel itself. An example of the effects of closely packed ions in a small region representing a calcium channel can be found in the work of Nonner *et al.* [92, 93] and validated by the equilibrium Monte Carlo simulations of Boda *et al.* [94, 95, 96].

An adequate treatment of the electrostatic properties of the systems of interest is crucial for the understanding of the dynamic properties of ion channels. We now consider the most common methodologies used to implement accurate and efficient electrostatic force-field schemes.

Three efficient approaches for electrostatic modeling of inhomogeneous systems are the Fast Multipole Method (FMM) [97, 98, 99] the Ewald summation method [100], and the Particle-Particle–Particle-Mesh (P^3M) method [83].

Conceptually, these three approaches are very similar [101] because they all consist of writing the total force acting on a charged particle i as the sum of a long-range and a short-range component:

$$\vec{F}_i = \vec{F}_i^{lr} + \vec{F}_i^{sr} \qquad [1]$$

The difference between the three methods is primarily in the calculation of the long-range force $\vec{F}_i^{lr}$. The FMM utilizes a multipole expansion to calculate the long-range force from particles that are far from particle i, while the short-range force is computed through the direct summation of the Coulomb force from particles omitted from the long-range calculation. Within the Ewald method, both the short-range and long-range components are calculated exactly from analytic expressions, where the short-range component is calculated in real space and the long-range contribution is calculated in reciprocal space. The P^3M formalism accounts for the short-range interactions by directly summing the coulombic particle-particle force in a small volume, while the long-range interaction is determined using the numerical solution of Poisson's equation on a discrete grid over the whole computational domain. Within both the Ewald and P^3M approaches, an overlap between the long-range and short-range domain exists and must be accounted for. This is discussed further in the section "Short-Range Interactions".

It is worth mentioning that in the original work of Hockney and Eastwood [83] on the P^3M approach, the solution of Poisson's equation is calculated in the reciprocal space with Green's functions. In this chapter, an iterative method to calculate the solution of Poisson's equation in real space is discussed. This approach is not commonly adopted for the particle-based simulation of liquid systems. The rather laborious implementation of robust three-dimensional Poisson solvers is probably one of the reasons for the lack of popularity of this approach, that we advocate nevertheless. For this reason, a section of this tutorial is devoted to the discussion of fast iterative methods for the solution of Poisson's equation in position space.

A detailed description of the components of the force $\vec{F}_i$ in Eq. 1 is given in the following sections, for the three different approaches.

2.1 Long-Range Interaction

This section is devoted to a discussion of the implementation of the long-range component within the FMM, Ewald summation and P^3M methods.

2.1.1 Multipole Expansion

The FMM [97, 98, 99] is based on a multipole series expansion of the long-range potential. The algorithm performance scales linearly with the number of particles [97], making FMM one of the most efficient approaches available for large systems.

As in the P^3M and Ewald summation methods, within the multipole method formalism the force is separated into a long- and short-range interaction, and the short-range component is resolved through a direct summation over the particle-particle interaction. The long-range component of the force on a generic particle i is computed as

$$\vec{F}_i^{lr} = -q_i \vec{\nabla} \Phi^{lr}(\vec{r}_i) \qquad [2]$$

where the long-range potential $\Phi^{lr}(\vec{r}_i)$ is computed by a pairwise summation of the charged particles excluded from the direct short-range calculation.

Given a set of point charges $\{j\}$, located inside a sphere of radius R centered about some origin, the long-range Coulomb potential at position $\vec{r}_i$ located outside the sphere (*i.e.* $|\vec{r}_i| > R$) can be written in spherical coordinates as,

$$\Phi^{lr}(\vec{r}_i) = \frac{1}{4\pi\epsilon_0\epsilon} \sum_{l=0}^{l_{max}} \sum_{m=-l}^{l} \frac{1}{2l+1} \frac{M_{lm}}{r_i^{l+1}} Y_{lm}(\theta_i, \phi_i) \qquad [3]$$

where the moments of the expansion are given by

$$M_{lm} = \sum_j q_j r_j^l Y_{lm}^*(\theta_j, \phi_j) \qquad [4]$$

and Y_{lm} and Y_{lm}^* are spherical harmonics [102]. A cutoff distance l_{max} has been introduced in Eq. 3 resulting in an error of order $O(r/R)^{l_{max}+1}$ [97]. Although the multipole expansion is generally written in spherical coordinates, Cartesian coordinates have also been used for the computation of the potential energy function [103, 104]. The representation in spherical coordinates is argued to produce a more efficient implementation than the Cartesian representation [105, 106].

Within the "cellular" version of the multipole method, the computational domain is discretized into a set of rectangular grid cells and the moments of the multipole expansion are computed and stored at each cell. The multipole expansion is only valid for particles that are separated by at least one grid cell [103], therefore the long-range part of the potential at a position $\vec{r}_i$ is calculated by summing the contributions from all the non-neighboring cells. An improvement of this approach is to use a hierarchy of grids with different cell sizes [107] that allows for the consolidation of cells into progressively larger groups as the distance between the position $\vec{r}_i$ and the cells increase. This coarsening scheme allows for the reduction of the total number of distant cells used in the calculation, and is based on the assumption that the distant charge distribution interacts less intensely than the close one [105]. The accuracy of the calculation remains constant if the ratio between the cell size and the distance is kept constant [106].

The FMM typically makes use of a local Taylor expansion to further improve the algorithmic efficiency [97]. The difference between the multipole expansion calculated in two different points laying in the same grid cell is assumed to be very small, thus justifying the use of a Taylor series expansion of the potential about the center of the grid cell. The coefficients of the Taylor expansion for each grid cell are calculated once and then evaluated for the position of each individual particle within a given grid cell.

The treatment of boundary conditions can be incorporated in the FMM scheme easily. Periodic boundary conditions as well as Dirichlet, Neumann and mixed conditions [98] can be accounted for. The FMM approach has been shown to be more efficient than the Ewald summation method (see the next section) but it results in code that is only faster than P^3M methods for nonphysically high numbers of particles [108]. Finally, it is worth noting that the FMM is applicable to all problems involving an r^{-n} pairwise potential [98].

2.1.2 Ewald Summation

The Ewald summation method was originally developed as an efficient way to calculate the long-range interactions in ionic crystals [100], and has become one of the most commonly used methods for modeling electrostatic properties in periodic structures [109], particularly for molecular dynamics simulations [110].

The electrostatic potential energy in a charged system can be written as the summation of all the pairwise coulombic interactions between charges. In a periodic array, this also includes the interaction with the infinite number of replica charges generated by the periodic repetition of the simulated system. The series of coulombic terms converges very slowly and the solution depends on the order of the summation, *i.e.* the series is conditionally convergent.

The Ewald formalism is based on a decomposition of the conditionally convergent series into two sums that individually have superior convergence properties. The method involves the addition of an appropriately shaped charge distribution to each charged particle having the same magnitude as the particle but of opposite sign. This charge distribution effectively screens the interactions with neighboring charges, resulting in a series that is limited to a short-range domain which in turn makes the resulting summation converge rapidly. To counteract the effects of the artificial charge distribution, a second charge distribution with the same magnitude and same sign as the original point charge is also included for each point charge. If this new charge distribution is smooth, the second summation that accounts for it can be Fourier-transformed and solved

efficiently in reciprocal space. From the physical viewpoint, this second summation recovers the long-range interactions that were screened out by introducing the first artificial charge distribution. The two series can then be combined to recover the potential energy due to the original point charges.

The traditional Ewald summation approach is generally presented in terms of the potential energy of the system. However, the force acting on a given particle is the quantity used by computational approaches, such as molecular dynamics and Brownian dynamics. Therefore, the derivation of the forces (instead of the potential energies) is required and how these forces are determined is described below.

The exact representation of the long-range component of the force is calculated in the reciprocal space using the Fourier transform. In three-dimensions the Fourier transform pairs are given by

$$f(\vec{r}) = V^{-1} \sum_{\vec{k}} \tilde{f}(\vec{k}) e^{\mathrm{i}\vec{k}\cdot\vec{r}} \qquad [5]$$

and

$$\tilde{f}(\vec{k}) = \int_V f(\vec{r}) e^{-\mathrm{i}\vec{k}\cdot\vec{r}} d\vec{r} \qquad [6]$$

where $V = L_x \times L_y \times L_z$ is the three-dimensional unit cell in real space, and the components of the vector $\vec{k}$ in the reciprocal space are restricted to the values $k_x = \frac{2\pi l}{L_x}$, $k_y = \frac{2\pi m}{L_y}$, and $k_z = \frac{2\pi n}{L_z}$, where l, m and n are integers.

The force acting on a charge distribution i can be written as

$$\vec{F}_i^{lr} = -\int q_i S(|\vec{r} - \vec{r}_i|) \vec{\nabla} \Phi(\vec{r}) d\vec{r} \qquad [7]$$

where $\vec{r}_i$ is the position of the center of the distribution and S is the shape of the distribution [102]. This integral representation is defined over one real space unit cell and an extra sum is made over each additional structure to include multiple periodic cells. Within the Ewald approach, the added charge distribution is generally (but not always) modeled with a Gaussian function [108]:

$$S(r) = \left(\frac{\alpha^2}{\pi}\right)^{3/2} e^{-\alpha^2 r^2} \quad [8]$$

where α determines the width of the charge distribution, and the Fourier transform of the Gaussian charge distribution is

$$S(|\vec{k} - \vec{k}_j|) = \frac{\alpha^2 V}{\sqrt{8\pi}} e^{\mathrm{i}\vec{k}\cdot\vec{r}_j} e^{-k^2/4\alpha^2} \quad [9]$$

The use of a Gaussian distribution is not required, and other functions have been used in the Ewald summation method [111]. For the sake of simplicity, the following derivation is limited to the use of Eq. 8.

The potential can be written in terms of the charge distribution by first applying the Fourier transform to Poisson's equation:

$$k^2 \tilde{\Phi}(\vec{k}) = -\frac{\tilde{\rho}(\vec{k})}{\epsilon\epsilon_0} \quad [10]$$

where the total charge density is given by all the remaining charges in the series:

$$\tilde{\rho}(\vec{k}) = \sum_{j \neq i} q_j \tilde{S}(|\vec{k} - \vec{k}_j|) \quad [11]$$

The potential in real space is then written as,

$$\Phi(\vec{r}) = -\frac{1}{V\epsilon\epsilon_0} \sum_{\vec{k}\neq 0} \frac{\tilde{\rho}(\vec{k})}{k^2} e^{\mathrm{i}\vec{k}\cdot\vec{r}} \quad [12]$$

$$= -\frac{1}{V\epsilon\epsilon_0} \sum_{\vec{k}\neq 0} \sum_{j\neq i} \frac{q_j}{k^2} \tilde{S}(|\vec{k} - \vec{k}_j|) e^{\mathrm{i}\vec{k}\cdot\vec{r}} \quad [13]$$

By substituting the equations for the potential into Eq. 7 and integrating over $\vec{r}$ one has

$$\vec{F}_i^{lr} = \frac{q_i}{\epsilon\epsilon_0 V} \sum_{j\neq i} q_j \sum_{\vec{k}\neq 0} \frac{\mathrm{i}\vec{k}}{k^2} S(|-\vec{k} - \vec{k}_i|) S(|\vec{k} - \vec{k}_j|) \quad [14]$$

the real part of which gives the final expression for the long-range component

of the force:

$$\vec{F}_i^{lr} = \frac{4\pi q_i}{\epsilon\epsilon_0 V} \sum_{j \neq i} q_j \sum_{\vec{k} \neq 0} \frac{\vec{k}}{k^2} e^{-k^2/4\alpha^2} sin(\vec{k} \cdot \vec{r}_{ij}) \quad [15]$$

where $\vec{r}_{ij} = \vec{r}_i - \vec{r}_j$.

The conventional Ewald summation method works well for simulations of small periodic systems, but the computation can become prohibitively expensive [112] when large systems are involved, in which the particle number exceeds 10^4 . Several numerical techniques have been used to enhance the performance of the traditional Ewald method with mixed results. For example, look-up tables and polynomial approximations [101] have been suggested. The algorithmic performance can also be optimized through the parameter α [113, 114], which determines both the extension of the short-range interaction and the allowable cutoff of the summation over the reciprocal space vectors [108]. Calculating the reciprocal sum is often the most efficient component of the algorithm and α can be chosen to minimize the portion of the summation performed over real space [113, 115]. Once the optimal value of α is determined, the performance of the approach can be significantly improved by implementing fast Fourier transform (FFT) algorithms to solve the summation in reciprocal space. The version of the Ewald summation based on these procedures is called the particle-mesh Ewald (PME) method [112, 116]. The reciprocal sum is then defined on a discretization grid by using a piecewise interpolation scheme to assign the charge density to grid-points used to evaluate the force (or potential) with FFT.

2.1.3 Poisson Solver in Real Space

Another possible approach for the computation of the long range force $\vec{F}_i^{lr}$ consists of assigning the charge density to the points of a generally inhomogeneous finite-difference grid, solving Poisson's equation [102], and differentiating the potential:

$$\vec{F}^{lr}(\vec{r}_p) = -q\vec{\nabla}\Phi(\vec{r}_p) \quad [16]$$

where $\vec{F}^{lr}(\vec{r}_p)$ and $\Phi(\vec{r}_p)$ represent the force and the electrostatic potential, respectively, at the grid point p located at $\vec{r}_p$. This component of the force also accounts for external boundary conditions, dielectric discontinuities, and fixed charges. The force $\vec{F}_i^{lr}$ on the ion i at the specific position $\vec{r}_i$ is then computed by an appropriate interpolation scheme.

To solve Poisson's equation on a grid, a charge assignment scheme must be devised that builds a charge distribution from the ionic coordinates. Furthermore, once the electrostatic field has been computed on the grid (from the solution of Poisson's equation) the force must be interpolated back to each ion location in a way that is consistent with the original charge assignment scheme. In other words, a geometric shape is assigned to each ionic charge though a space-dependent weighting function $W(\vec{r})$ [83], and the geometrical relation between the charge shape and the discretization grid is accounted for in all the transformations used to transfer quantities (i.e. charge and force) to and from the mesh centered at $\vec{r}_p$.

The generalized algorithm to accomplish this follows the treatment of Hockney [83]:

1. *Assign charge:*

$$\rho(\vec{r}_p) = \frac{1}{V_p} \sum_i^{N_p} q_i W(\vec{r}_i - \vec{r}_p) \qquad [17]$$

2. *Solve Poisson's equation:*

$$\vec{\nabla} \cdot \epsilon_r \vec{\nabla} \Phi(\vec{r}_p) = -\frac{\rho(\vec{r}_p)}{\epsilon_0} \qquad [18]$$

3. *Calculate electric field:*

$$\vec{E}(\vec{r}_p) = -\vec{\nabla} \Phi(\vec{r}_p) \qquad [19]$$

4. *Interpolate force:*

$$\vec{F}_i^{lr} = \sum_p^{N_p} q_i W(\vec{r}_i - \vec{r}_p) \vec{E}(\vec{r}_p) \qquad [20]$$

where V_p and N_p are the volume of the grid and number of particles in the grid,

respectively. It should be noted that the same function $W(\vec{r})$ must be used both for the charge assignment and for the force interpolation, because the use of a mixed scheme can result in a nonphysical self-force of the particle upon itself. The three most common charge assignment schemes are called the nearest-grid point (NGP), the cloud-in-cell (CIC) and the triangular-shaped cloud (TSC) schemes [83], and represent the particle as a point charge, an uniformly charged sphere, and a sphere with a linearly decreasing density, respectively. The choice of the weighting function depends on the properties of the system. Once a shape has been chosen for the charge, the corresponding weighting function is determined by the following integral:

$$W(\vec{r} - \vec{r}_p) = \int_{V_p} S(\vec{r'} - \vec{r}) d\vec{r'} \qquad [21]$$

where the function $S(\vec{r})$ represents the shape of the charge "cloud" associated with the particle. In one dimension, the weighting functions computed from Eq. 21 are given for the three charge shapes by the following relations:

$$W_{NGP}(x) = \begin{cases} 1 & \left|\frac{x}{H}\right| \leq \frac{1}{2} \\ 0 & \text{else} \end{cases} \qquad [22]$$

$$W_{CIC}(x) = \begin{cases} 1 - \left|\frac{x}{H}\right| & \left|\frac{x}{H}\right| \leq 1 \\ 0 & \text{else} \end{cases} \qquad [23]$$

$$W_{TSC}(x) = \begin{cases} \frac{3}{4} - \left|\frac{x}{H}\right|^2 & \left|\frac{x}{H}\right| \leq \frac{1}{2} \\ \frac{1}{2}\left(\frac{3}{2} - \left|\frac{x}{H}\right|\right)^2 & \frac{1}{2} \leq \left|\frac{x}{H}\right| \leq \frac{3}{2} \\ 0 & \text{else} \end{cases} \qquad [24]$$

where H is the mesh size. For the three dimensional case, the weighting function is obtained as follows:

$$W(\vec{r}) = W(x)W(y)W(z) \qquad [25]$$

In agreement with the work of Hockney [83], the TSC weighting function is usually the optimal compromise between accuracy and computational performance for the systems discussed in this chapter.

Using a Poisson solver for the long-range interaction results in two main advantages: *1)* the possibility to impose boundary conditions through externally applied potentials, and *2)* the ability to simulate systems with arbitrary ionic concentrations at the boundaries.

2.1.4 Finite Difference Iterative Schemes

A numerical method is said to be direct when it finds a solution within a given precision, and with a given accuracy, in an initially known number of operations. The time required to solve a differential equation is then well known *a priori*, and it is *independent* of the initial or boundary conditions of the problem. Iterative methods, on the other hand, are based on a sequence of approximations to the required solution, starting from an initial guess that converge to the solution. The number of operations, and the time required by these latter methods' are initially unknown since they depend on the initial guess and may vary dramatically as a function of the parameters of the problem itself.

The self–consistent nature of the simulation approaches described in this chapter requires frequent solutions of Poisson's equation; the sequential potential profiles from one step to the next are very similar to each other since the changes in the charge distribution between two consecutive solutions are very small (but very important for the particle dynamics). The current potential profile can thus generally be used as a good initial guess for the next solution, making iterative methods a natural choice within the framework of self–consistent simulation programs. In addition, memory issues [117] (other than pure performance) make the choice of iterative methods appealing in the field of ion channel simulations.

We now present and discuss the basic steps in standard stationary linear iterative methods [118] needed to compute the electrical forces. The present

discussion concentrates on the general representation of the two–dimensional Poisson's equation for simplicity,

$$\nabla^2 \Phi = f(x, y) \qquad [26]$$

Employing finite differencing on a set of grid points defining the discrete grid denoted by Ω_n, this elliptic differential equation is transformed into an algebraic matrix equation of the form,

$$A\mathbf{u} = \mathbf{f} \qquad [27]$$

where the vector $\mathbf{u}$ denotes the solution, the matrix A represents the Laplace operator, and $\mathbf{f}$ is a generic forcing function.

Within the iterative framework, a sequence of approximations $\mathbf{v}^0, \mathbf{v}^1, ..., \mathbf{v}^n, ...$ to $\mathbf{u}$ is constructed that converges to $\mathbf{u}$ [118]. Let $\mathbf{v}^i$ be the approximation to $\mathbf{u}$ after the i^{th} iteration. Because the exact solution $\mathbf{u}$ of Eq. 27 is unknown, one may define the *residual*,

$$\mathbf{r}^i = \mathbf{f} - A\mathbf{v}^i \qquad [28]$$

as a computable measure of the deviation of $\mathbf{v}^i$ from $\mathbf{u}$. Next, the *algebraic error* $\mathbf{e}^i$ of the approximation $\mathbf{v}^i$ is defined by,

$$\mathbf{e}^i = \mathbf{u} - \mathbf{v}^i \qquad [29]$$

Subtracting Eq. 28 from Eq. 27 and rearranging terms, it is easily shown that $\mathbf{e}^i$ obeys the so–called *residual equation*,

$$A\mathbf{e}^i = \mathbf{r}^i \ . \qquad [30]$$

Iterative methods can be interpreted as applying a *relaxation operator* to $\mathbf{v}^i$ so as to obtain a better approximation $\mathbf{v}^{i+1}$ by reducing of the error $\mathbf{e}^i$ related to $\mathbf{v}^i$. In this way, the sequence of approximations $\mathbf{v}^0, \mathbf{v}^1, ..., \mathbf{v}^n, ...$ is "relaxed" to

the solution $\mathbf{u}$.

The expansion of the matrix equation (Eq. 27) gives the following relation:

$$u_k = \frac{-\sum_{\substack{j=1 \\ j\neq k}}^{n} a_{kj}u_j + b_k}{a_{kk}}, \quad k = 1, 2, ...n \quad ; \quad a_{kk} \neq 0 \qquad [31]$$

In Jacobi's method [119], the sequence $\mathbf{v}^0, \mathbf{v}^1, ..., \mathbf{v}^n, ...$ is then computed by,

$$v_k^{(i+1)} = \frac{-\sum_{\substack{j=1 \\ j\neq k}}^{n} a_{kj}v_j^{(i)} + b_k}{a_{kk}}, \quad k = 1, 2, ...n \quad ; \quad a_{kk} \neq 0 \qquad [32]$$

It should be noted that one does *not* use the improved values until after a *complete* iteration, within this method. In the closely related Gauß–Seidel's method [118] the values are used as soon as they are computed. One then has,

$$v_k^{(i+1)} = \frac{-\sum_{j=1}^{k-1} a_{kj}v_j^{(i+1)} - \sum_{j=k+1}^{n} a_{kj}v_j^{(i)} + b_k}{a_{kk}}, \quad k = 1, 2, ...n \quad ; \quad a_{kk} \neq 0. \quad [33]$$

Note that here only one approximation for each v_k needs to be stored at a time. Proofs and discussions about the convergence properties of iterative methods can be found in Young [118] and Dahlquist and Björck [119].

It is often possible to obtain a substantial improvement of the convergence rate by a simple modification of the Gauß–Seidel's method. Note that, following the definition of the residual given in Eq. 28, Eq. 33 can be written as $v_k^{(i+1)} = v_k^{(i)} + r_k^{(i)}$, where $r_k^{(i)}$ is the current residual of the k-th equation:

$$r_k^{(i)} = \frac{-\sum_{j=1}^{k-1} a_{kj}v_j^{(i+1)} - \sum_{j=k}^{n} a_{kj}v_j^{(i)} + b_k}{a_{kk}}, \quad k = 1, 2, ...n \quad ; \quad a_{kk} \neq 0. \qquad [34]$$

The iterative method

$$v_k^{(i+1)} = v_k^{(i)} + \omega r_k^{(i)} \qquad [35]$$

is then the so–called *successive overrelaxation* (SOR) method. Here ω, the *relaxation parameter*, should be chosen so that the rate of convergence is maximized. For $\omega = 1$, the SOR approach reduces to the Gauß–Seidel's method. The SOR method has been shown to converge *only* for $0 < \omega < 2$ [119].

The rate of convergence of SOR is often higher than when using the Gauß–Seidel method, and, the additional computational load associated with SOR is negligible. However, the value of ω depends on the grid spacing, the geometrical shape of the domain, and the type of boundary conditions imposed on it [120]. Efforts have been undertaken to find an approach that predetermines the optimal value of ω as a function of the discretization scheme [121, 122]. Some improvements in the convergence rate have also been obtained by modifying the processing order of the grid points [83, 123]. In spite of this, the performance of the SOR approach is inadequate for the implementation of real space Poisson solvers for the simulation of systems discretized on a large number of grid points such as the ones described in this document.

2.1.5 The multi-grid method

In the previous section we discussed the basic theory of the classical iterative solution to elliptic problems. The multi-grid method allows for a dramatic performance improvement of standard iterative approaches such as the SOR method. The basic principles of its operations are briefly introduced in the following section.

Error reduction in classical iterative methods Iterative methods for the solution of large sparse systems of equations have been presented above. These methods produce, by iteration, a sequence of approximations to the required solution which converge to the solution itself. This process progressively reduces the error related to each approximation. A given approximation is then accepted

as the solution when the deviation from the previous approximation (or some norm of it) is smaller than a predefined threshold. Therefore, an analysis of the error expressed in Eq. 30 as a function of the iteration number (or of the required computer time, since the the number of operations per iteration is constant) can provide a useful indication of the solver performance.

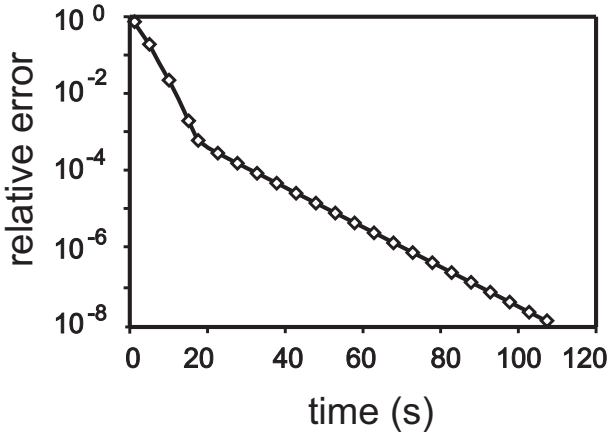

Figure 6: Error reduction rate of the successive overrelaxation method. The smaller slope of the curve for small relative error values indicates the poor performance of solvers based on this method.

The absolute value of the maximum relative error is plotted versus the CPU time for a SOR solver in Fig. 6. The slope of the curve gives an indication of the performance of the solver: the initial error reduction is very fast, as confirmed by the steep slope of the curve in the upper left corner of the plot. As the error becomes smaller, the slope is less pronounced, showing a dramatic degradation of the performance. The values of the error that are usually acceptable in particle–based simulations lie in this low performance region, *i.e.* typically in the range $[10^{-5}, 10^{-7}]$. The reason for the performance degradation shown in Fig. 6 can be understood easily through a spectral analysis of the error before and after a relaxation sweep.

Figure 7 shows, in the upper plots, a schematic representation of the error before (left) and after (right) a single iteration on a unidimensional domain. In

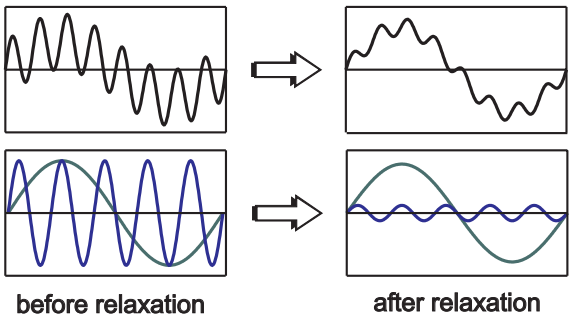

Figure 7: Schematic representation of the relative error of an iterative method after a relaxation sweep. The lower plots show that the low frequency Fourier component of the error is less reduced than the high frequency one.

the lower plots, the corresponding Fourier components of the error are depicted; in this simplified picture only two Fourier components are shown. Application of one relaxation sweep affects only the high frequency component, which is much more reduced in amplitude than is the low–frequency, long wavelength component. Thus, the two–slope curve shown in Fig. 6 can be explained as follows: the relaxation operator of the iterative method is efficient in reducing only *some* of the Fourier components of the error. Its error reduction rate slows down because the remaining components (the ones with long wavelengths) are not reduced as efficiently. This difference in the error reduction is due to the grid spacing: those components of the error with a wavelength comparable to the grid spacing are reduced more efficiently by the relaxation operator.

Multi-grid basics The basic idea of the multi–grid approach is to simultaneously employ *different* length scales to efficiently reduce the error. Specifically, one solves Eq. 30 exactly on a grid Ω_{n-1} that is *coarser* than the initial given grid Ω_n. The resulting value of $\mathbf{e}^i$ is an approximation that is used to *correct* the previous approximation $\mathbf{v}^i$ that has been determined on the original grid Ω_n,

$$\mathbf{v}^{i+1} = \mathbf{v}^i - \mathbf{e}^i \qquad [36]$$

The advantage of this approach can be understood by considering the Fourier expansion of the error $\mathbf{e}^i$ shown in Fig. 7. The long wavelength components of $\mathbf{e}^i$ are only slightly reduced on the fine grid because their spatial extent exceeds the range of the relaxation operator. The use of a coarser grid renders those components to have an effectively shorter wavelength and thus making those long wavelength components "visible" to the relaxation operator. This improves the convergence of the solver dramatically, as compared to a single–grid based relaxation scheme, such as the SOR.

The simplest version of the multi–grid algorithm is the so–called *two–grid iteration* employing only two grid levels. In the i^{th} iteration, the procedure starts from the approximation $\mathbf{v}^i$ of $\mathbf{u}$ in Eq. 27 and the following five steps are performed:

1. Smooth $\mathbf{v}^i$ on the grid Ω_n by applying some suitable relaxation scheme, called *pre–smoothing*.

2. Compute the residual according to Eq. 28 and transfer it to the coarser grid Ω_{n-1}. This step is called *restriction*.

3. Solve Eq. 30 exactly on the grid Ω_{n-1}.

4. Interpolate the resulting $\mathbf{e}^i$ to the finer grid Ω_n. This step is called *prolongation*. Subsequently, calculate $\mathbf{v}^{i+1}$ from Eq. 36.

5. Smooth $\mathbf{v}^{i+1}$ on the grid Ω_n by applying some relaxation method, termed *post–smoothing*.

It is possible to extend the two–grid algorithm to a sequence of grids that are increasingly coarse, since Eq. 30, applied on the grid Ω_{n-1}, has *the same form* as Eq. 27 on Ω_n. This is achieved by recursively applying the complete algorithm (step 1 through 5) at step 3. The recursion scheme is stopped when the coarsest grid Ω_0 is reached. At that grid level, Eq. 30 is solved exactly. Since this grid

usually contains only a few points, this can be done easily. This multi–scale algorithm defines one complete *multi–grid iteration* (labeled by the superscript i). The whole procedure is then repeated until the required convergence threshold is reached.

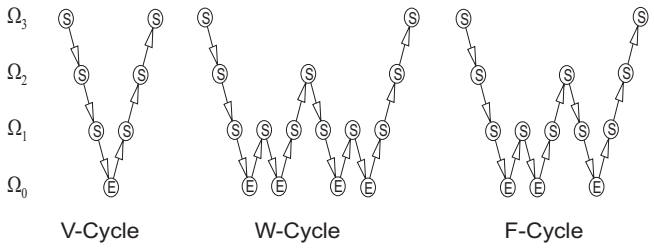

Figure 8: Standard multi–grid structure for a V–, W–, and F–cycle. In this figure, the number of grid levels is four, the circles represent a *S*moothing operation or an *E*xact solution, the arrows indicate prolongation (upward) and restriction (downward) operations. Ω_0 represents the coarsest, and Ω_3 the finest grid.

The above discussion of the multi–grid iteration refers to a cyclic structure called V–cycle (see Fig. 8). More generally, one may define the multi–grid iteration as the recursive application of γ two–grid cycles at any grid level, the V–cycle being characterized by $\gamma = 1$. The case $\gamma = 2$ is called W–cycle. It is possible to use any number γ of two–grid cycles at each level, obtaining better convergence at the cost of increased complexity of the algorithm. A special cycle, the so–called F–cycle, is also shown in Fig. 8. It is important because its structure often optimizes the trade–off between pure performance and complexity. The F–cycle on Ω_i is recursively defined as follows [124]: its coarse grid part consists of an F–cycle on Ω_{i-1}, followed by a V–cycle on Ω_{i-1}. An F–cycle on the coarsest grid Ω_0 is just a V–cycle.

Finally, it should be noted that the multi–grid method can be used as either an iterative process or as a direct solver (the so–called *full multi–grid* or *nested iteration* method [125]).

Algorithmic details on the multi–grid method can be found in the excellent works of Hackbusch [125] and Brandt [126, 127]. It should be noted that

the multi–grid approach can be easily applied to adaptive non-tensor-product grids [126, 127], allowing for variable resolution in regions of the computational domain where the charge concentration is high. A discretization scheme based on adaptive grids can result in a further increase in performance when simulating highly inhomogeneous systems such as biological membranes or complex proteins.

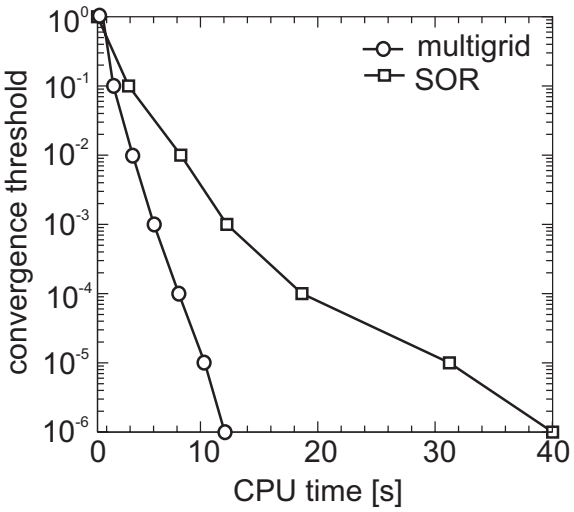

Figure 9: Comparison of the CPU time required to solve Poisson's equation with the multi–grid and SOR method. The computational domain consists of a 65x65x65 homogeneous mesh.

The SOR method for solving Poisson's equation in ion-channel applications is not advocated here because of its slower convergence compared to the multi–grid approach, and, because of its inefficiency for large problems. It is recognized, however, that the extreme simplicity of the SOR algorithm makes it an attractive choice. A typical SOR solver can be implemented with a few tens of lines of code, while our 3D multi–grid solver is several thousand lines long.

2.2 Short-Range Interactions

The short range force is written as three terms,

$$\vec{F}_i^{sr} = \vec{F}_i^C + \vec{F}_i^W + \vec{R}_i \qquad [37]$$

where $\vec{F}_i^C$ is the coulombic force due to all the particles within a predefined short-range domain, $\vec{F}_i^W$ represents the effects of the van der Waals forces, and, where $\vec{R}_i$ is a "reference force" [83] that corrects the double counting of charges due to the overlap between the short-range and long-range domains occurring in both the Ewald and P^3M methods. No overlap exists within the FMM formalism, so the reference force is null in such a scheme. The forces in Eq. 37 are expressed as follows:

$$\vec{F}_i^C = \sum_{j \neq i}^{\Lambda_i} \frac{q_i q_j}{4\pi\epsilon_r\epsilon_0 |\vec{r}_i - \vec{r}_j|^2} \hat{r}_{ij} \qquad [38]$$

$$\vec{F}_i^W = \begin{cases} \displaystyle\sum_{j \neq i}^{\Lambda_i} \frac{24\epsilon_{ij}}{|\vec{r}_i - \vec{r}_j|} \left[2\left(\frac{\sigma_{ij}}{|\vec{r}_i - \vec{r}_j|}\right)^{12} - \left(\frac{\sigma_{ij}}{|\vec{r}_i - \vec{r}_j|}\right)^{6} \right] \hat{r_{ij}} & \textit{Lennard-Jones} \\ \displaystyle\sum_{j \neq i}^{\Lambda_i} \frac{\beta_{ij}\,|q_i q_j|}{4\pi\epsilon |\vec{r}_i - \vec{r}_j|(p+1)} \left(\frac{s_i + s_j}{|\vec{r}_i - \vec{r}_j|}\right)^{p} \hat{r_{ij}} & \textit{inverse power} \end{cases} \qquad [39]$$

$$\vec{R}_i = -\sum_{j \neq i}^{\Lambda_i} \frac{q_i q_j}{4\pi\epsilon_r\epsilon_0} \iint S(\vec{r}_1) S(\vec{r}_2 - \vec{r}_{ij}) \frac{(\vec{r}_1 - \vec{r}_2)}{|\vec{r}_1 - \vec{r}_2|^3} d\vec{r}_1 d\vec{r}_2 \qquad [40]$$

where Λ_i is the domain of the short-range interaction (see below), ϵ_r is the relative dielectric constant, ϵ_0 is the permittivity of vacuum, q is the charge, and $\vec{r}_{ij}$ is the distance between ions.

The van der Waals force $\vec{F}_i^W$ is often modeled with the Lennard-Jones function or by an inverse power relation [128]. The former is based on the two fitting

parameters σ_{ij} and ϵ_{ij}, representing respectively the maximum attraction distance and the strength of the interaction [129]. For ions of different species, the Lennard-Jones parameters are typically calculated by combining the values of the individual species [129],

$$\sigma_{ij} = \frac{1}{2}(\sigma_i + \sigma_j), \quad \text{and,} \quad \epsilon_{ij} = \sqrt{\epsilon_i \epsilon_j} \qquad [41]$$

In the expression of the inverse power law, β_{ij} is an adjustable parameter, s_i is the radius of the ith particle, and p is a hardness parameter that also represents the interaction strength. A comparison of the inter-ionic potential profile for the two different pair potential schemes in an aqueous KCl solution is shown in Fig. 10. The parameters used for the short range potentials are taken from Im *et al.* [130] for the Lennard-Jones function and from Hockney [83] for the inverse power relation.

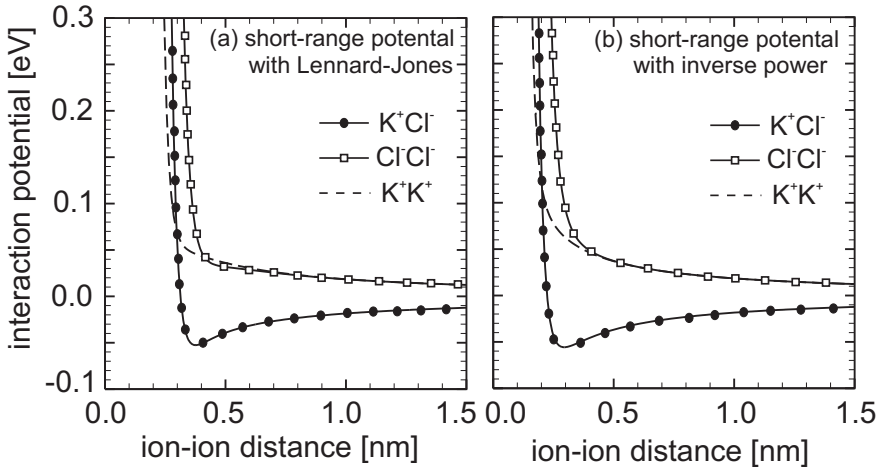

Figure 10: Comparison of short range Lennard-Jones and inverse power potential for K^+ and Cl^- in aqueous solution.

The final component of the particle-particle force is the reference force $\vec{R}_i$, which depends on the shape S of the ionic charge. As previously stated, within the P^3M approach, the particle-particle portion of the force is calculated for

ions within the relatively small spherical region Λ_i. The role of the reference force is to correct for the overlap between Λ_i and the entire system over which the mesh force $\vec{F}_i^{lr}$ is calculated. In other words, the sources of the electrostatic force acting on a given charged particle are classified as "far sources" (including boundary conditions) that are accounted for efficiently by the solver for the long-range interaction, and "close sources" generating forces that are not resolved by the solver and must be computed by the more CPU expensive particle-particle scheme. The domain Λ_i defines the high resolution region around a given ion. For obvious reasons, the computation of the long range interactions can not be obtained by subtracting the charges within Λ_i – this would indeed require a full solution for each particle at each iteration – so *the effect* of those sources is subtracted from the potential distribution *after* the solution has been obtained. This correction is accomplished by the reference force.

Clearly, the size of the region Λ_i should be chosen as small as possible based on performance considerations. The key aspect that limits the minimum size of Λ_i is the size of the ionic charge used for the charge assignment scheme (see "Poisson Solver in Real Space"). As stated above, the charge distribution is computed by assigning a "cloud" of charge to each individual ion. The cloud has a specific geometric shape and a predefined charge density. When calculating the total force on a given ion i, all the charged particles $j \neq i$ whose charge cloud is overlapping with that of i are considered "close sources" of the electrostatic force, and must be included in the domain Λ_i.

For example, if the chosen ionic electrostatic shape S is a sphere with an uniformly decreasing charge density, the corresponding weighting scheme is the TSC [83]:

$$S(r) = \begin{cases} \frac{3}{\pi r_c}\left(r_c - r\right) & r_c \leq r \\ 0 & \text{else} \end{cases} \qquad [42]$$

where r_c is the radius of the spherical charge cloud. In this case, the natural choice for the minimum cutoff radius that defines the short-range region Λ_i is

twice r_c. The reference force is then found analytically by substituting the shape function $S(r)$ into Eq. 40:

$$R(r) = \frac{q_i q_j}{4\pi\epsilon_r\epsilon_0} \begin{cases} \frac{4}{35r_c^2}(224\zeta - 224\zeta^3 + 70\zeta^4 + 48\zeta^5 - 21\zeta^6) & 0 \le \zeta \le 1 \\ \frac{4}{35r_c^2}(12/\zeta^2 - 224 + 896\zeta - 840\zeta^2 + 224\zeta^3 & \\ \quad +70\zeta^4 - 48\zeta^5 - 7\zeta^6) & 1 \le \zeta \le 2 \\ \frac{1}{r^2} & \text{else} \end{cases} \quad [43]$$

where $\zeta = r/r_c$. To reduce the computational burden, the reference force is tabulated as a function of the distance between ion pairs as suggested by Hockney [83] and subsequently by Wordelman [131] during initialization.

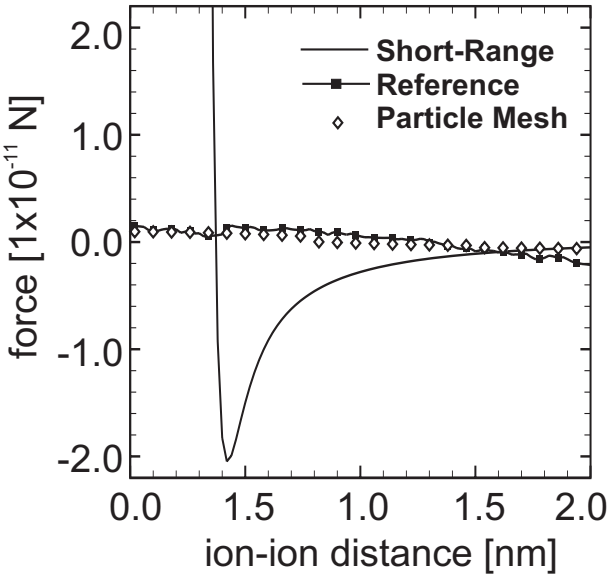

Figure 11: Components of the force inside the short-range domain calculated between two ions of opposite charge in a 500 mM solution of KCl with no bias.

The components of the force between an anion and a cation inside the short-range domain ($2r_c$=2 nm) are shown in Fig. 11 as a function of the inter-ionic

separation. The two ions are placed in a 500 mM KCl solution, with no external bias. As expected, the reference force and mesh force have the same amplitude, and therefore will cancel within the short-range domain.

Within the Ewald approach, the charge distribution is defined as a Gaussian function (see Eq. 8), and the sum of the direct Coulomb force and reference force can be written as an analytic expression. The final expression for the short-range interaction is then

$$\vec{F}_i^{sr} = \vec{F}_i^W + \frac{q_i}{4\pi\epsilon\epsilon_0} \sum_{j \neq i} q_j \left(\texttt{erfc}[\alpha|\vec{r}_{ij}|] + \frac{2\alpha}{\sqrt{\pi}} |\vec{r}_{ij}| e^{-\alpha^2 r_{ij}^2} \right) \frac{\vec{r}_{ij}}{|\vec{r}_i - \vec{r}_j|^3} \qquad [44]$$

2.3 Boundary Conditions

Once the significant components of the system have been chosen, a computational domain is then defined to enclose them. The geometry of the simulation box must define a volume that realistically encloses the physics of the system, with boundary conditions mimicking the effects of the larger, real system being modeled. Within the ion channel framework, only a small fraction of the cellular lipid membrane is simulated; thus the dimension of the computational domain is minimized to reduce the computational burden. Consequently, the boundary conditions must be chosen carefully so that unwanted computational artifacts are not introduced into the simulation results.

The most popular, and somehow elegant, choice is to impose periodic boundary conditions on a parallelepiped-shaped domain. This approach is adequate for simulating bulk systems because it ensures continuity of the ionic flux and of the force field at the boundaries. It is also compatible with the algorithm that accounts for long-range electrostatic interactions in the Ewald summation method. However, the periodic boundary approach also has drawbacks that are sometimes difficult to address. The main problem involves the charge distribution within the computational domain. The source of this problem is due to the highly inhomogeneous ion charge distribution that generates far-reaching

electric fields. When a periodic boundary "cuts" the field distribution, significant perturbations are generated in the forces that drive the dynamics of the system; care must be taken in choosing the size of the periodic box. To validate the results obtained with periodic boundaries, Yang suggests running the same simulation on computational domains of different size; that way the presence of size-dependent artifacts can be deleted and then excluded [132]. Furthermore, periodic boundaries make it extremely difficult to simulate systems with inhomogeneous charge distributions at the boundary, such as those systems with different dielectric coefficients in different regions or with different solutions on either side of the membrane. Also, the common experimental practice of applying external potentials across the solution is difficult to reproduce in a periodic system.

The use of nonperiodic boundary conditions is also complicated, especially by the necessity for having a mechanism that effectively and realistically recirculates mobile components (ions and sometimes water molecules) that escape from the computational domain. The injection scheme is trivial in periodic systems, but is not at all obvious [133] for the nonperiodic systems.

Two main types of electrostatic boundary conditions are used in nonperiodic systems. The Dirichlet boundary condition fixes the value of the electrostatic potential, while the Neumann method sets the value of the normal component of the electric field [83]. One approach employed to regulate the injection of ions in nonperiodic systems is to use reservoirs of particles and a simple stochastic boundary that maintains a given concentration value in the entire system [134]. Ions are recycled from one side of the domain to the other whenever there is an imbalance due to a conduction event. It has been shown that the simple stochastic boundary method of constant injection gives very similar fluctuations in the particle number of regions of the computational domain far from the injecting boundaries [134]. This approach is simple and efficient, but has the drawback of not being able to handle concentration gradients. Rather than maintaining the concentration in the entire domain, another approach consists of simply fixing the concentration in the Dirichlet boundary cells, and injecting

particles to sustain this concentration. That way, the concentrations at different boundaries can be different.

A third approach [130] is to inject particles based on a grand canonical ensemble distribution. At each predetermined molecular dynamics time step the probability to create or destroy a particle is calculated and a random number is used to determine whether the update is accepted (the probability for both the creation and destruction of a particle must be equal to ensure reversibility). The probability function depends on the excess chemical potential and must be calculated in a way that is consistent with the microscopic model used to describe the system. In the work of Roux [130], a primitive water model is used, and the chemical potential is determined through an analytic solution to the Ornstein-Zernike equation using the hypernetted chain as a closure relation [72]. This method is very accurate from the physical viewpoint, but has a poorer CPU performance compared to simpler schemes based on constant injection rates because of the continuous calculation of the chemical potential.

3 Particle-Based Simulation

A key component of particle-based simulation methods involves the coupling of the dynamics of the charge carriers (ions) with the field of forces generated by the *external* boundary conditions as well as by the *internal* electrostatic interactions between the components of the system. This *self-consistent* coupling approach has been successfully employed for more than three decades in plasma simulations [135]. The adjective *self-consistent* refers to the fact that the forces due to the electrostatic interactions within the components of the system depend strictly on the spatial configuration of the components themselves, and must be updated continuously as the dynamics of the system evolves.

Self-consistency is achieved by periodically "freezing" the dynamics, and by updating the spatial force distribution. The dynamics is then resumed in the "updated" field of forces, which is assumed to be constant for a time Δt that, in the cases of interest, is usually on the order of a femtosecond. At the end of

Δt a new field is computed from the new charge distribution.

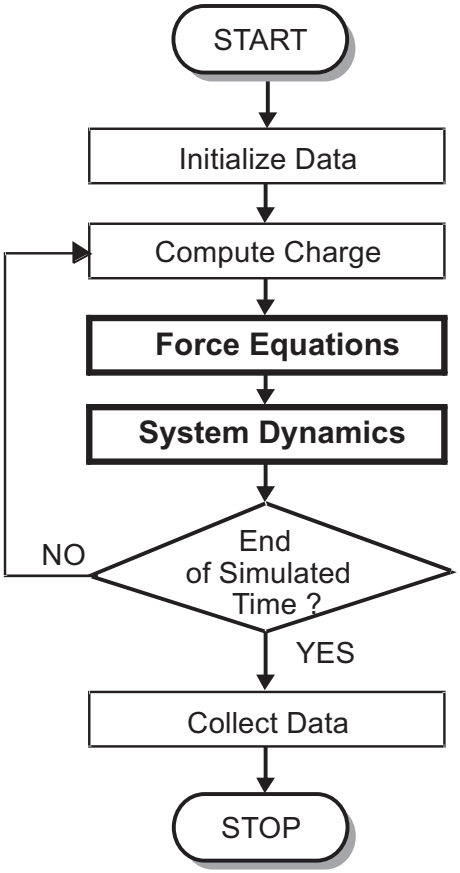

Figure 12: Flowchart of the self-consistent, particle-based algorithm.

The need for self-consistency between charge and force distributions is due to the spatial inhomogeneities of the systems under scrutiny. The long-range nature of the electrostatic interaction makes the relation between ionic concentration and field distribution highly non-linear [136, 137]. Significant differences in methodology for implementing the potential functions in simulation programs [138] exist. Figure 12 depicts the flowchart of a typical particle-based algorithm. The self-consistent aspect of the approach is enforced within the main iteration cycle, where the field of force and the ionic dynamics are contin-

uously coupled during the simulation.

The following section is devoted to two popular approaches for particle-based simulations of ionic charge transport in transmembrane proteins. The name used for the family of approaches to be discussed has its origin in the fact that at least some of the components of the system are represented as computer "particles", and their trajectories are tracked in phase-space. While mobile ions in solution are always modeled as particles, their dynamics can be Brownian or Newtonian based on the representation of the water solvent. When the effects of water on the system dynamics are modeled through macroscopic quantities such as the diffusion coefficient or the dielectric constant rather than by treating each atom (or collection of atoms)as a unique particle that exerts its influence on the system, we say that the solvent is treated implicitly, *i.e.*, we are implying in some way that the water is there influencing the system's dynamics. Alternatively, the solvent model is defined as being "explicit" if the water molecules are represented as separate entities, each obeying the laws of physics and thus influencing the system's dynamics.

3.1 Implicit Solvent: Brownian Dynamics

When the solvent is treated as a continuous dielectric background that interacts stochastically with the mobile ions, the ionic trajectories can be modeled with the Langevin formalism [139, 140]. In particular, the strict or full Langevin equation can be used, which assumes Markovian random forces and neglects correlations (both spatially and temporally) of the ionic motion:

$$m_i \frac{d\vec{v}_i(t)}{dt} = -m_i \gamma \vec{v}_i(t) + \vec{F}_i(\vec{r}_i(t)) + \vec{B}_i(t) \qquad [45]$$

where m_i is the reduced mass of the i^{th} ion, $\vec{v}_i(t)$ is its velocity at time t, γ is the friction coefficient (*i.e.,* the inverse of the ionic velocity relaxation time), $\vec{F}_i$ is the force on ion i due to all other particles in the system and boundary conditions (including internal dielectric discontinuities), and, $\vec{B}_i$ is a fluctuating force that mimics the molecular bombardment of water on the ion, and is modeled with

a Markovian random variable. The fluctuating force can therefore be written explicitly as,

$$\vec{B}(t) = \sqrt{2\gamma m k_B T}\dot{w} \qquad [46]$$

where a Gaussian white noise term is given by $\dot{w}$.

The Langevin equation is discretized temporally by a set of equally spaced time intervals. At predetermined times the ion dynamics is frozen, and the spatial distribution of the force is calculated from the vector sum of all its components, including both the long-range and the short-range contributions. The components of the force are then kept constant while the dynamics resumes under the effect of the updated field distribution. Self-consistency between the force field and the ionic motion in the phase-space is obtained by iterating this procedure for a desired amount of simulation time. The choice of the spatial and temporal discretization schemes plays a crucial role in terms of computational performance and model accuracy.

The integration scheme used for Eq. 45 is chosen based on fulfilling two requirements: maintaining energy stability and allowing for large time-steps. The latter requirement is related to the need to investigate system properties for the typically long biological time scales, which can be on the order of microseconds or more. Using long time-steps reduces the number of operations for each unit of simulated time, thus increasing the performance of the simulation code. Counteracting this is the requirement that the time-step must be small compared with the mean time between particle collisions. An excessively coarse time discretization would not account for rapid variations in the short-range force, and does not correctly account for its coulombic singularity. A large timestep typically results in a spurious heating of the particle ensemble that then becomes energetically unstable [83].

Two common implemented integration schemes for the Langevin equation are the standard first-order Euler scheme and the *Verlet-like* method by Gunsteren and Berendsen [141]. The later is a third order model that reduces to the

Verlet algorithm [142] when the friction coefficient in the Langevin equation is zero (see section on Explicit Solvent below). This approach by Gunsteren and Berendsen allows for a larger time-step as compared to the Euler method. Both schemes are discussed in the following sections, and a comparison is offered.

3.1.1 Particle Tracking: Euler Integration

The first order Euler integration scheme reduces the Langevin equation to

$$\vec{v}_i(t+\Delta t) = \vec{v}_i(t) - \Delta t\left[\gamma\vec{v}_i(t) - \frac{\vec{F}_i}{m_i} - \sqrt{\frac{2\gamma k_B T}{m_i \Delta t}}\vec{N}(0,1)\right] \qquad [47]$$

where Δt is the integration time-step and $\vec{N}(0,1)$ is a three dimensional Gaussian random variable with zero mean and variance of 1. The spatial trajectories are calculated with Newtonian mechanics. To represent the fluctuating force as a stationary Markovian, Gaussian process, the time-step duration Δt must be much smaller than the reciprocal of the friction coefficient γ in the Langevin equation (Eq. 45) [141]. This results in a fine (and computationally expensive) time discretization when ionic solutions are simulated.

3.1.2 Particle Tracking: Verlet-like Integration

The need for carrying out impractically short time-steps was addressed by Gunsteren and Berendsen [141] who accounted for the evolution of the fluctuating force during the integration time-step. In their method, the force on the i^{th} particle at time t_{n+1} is first expanded in a power series about the previous time t_n,

$$F_i(t_{n+1}) \sim F_i(t_n) + \dot{F}_i(t_n)(t_{n+1} - t_n) \qquad [48]$$

where $\dot{F}$ denotes the time derivative. The power series expansion is then substituted into Eq. 45, and the resulting solution of the Langevin equation is,

$$
\begin{aligned}
v_i(t_{n+1}) = v_i(t_n)e^{-\gamma\Delta t} &+ (m_i\gamma)^{-1}F_i(t_n)(1-e^{-\gamma\Delta t}) \\
&+ (m_i\gamma^2)^{-1}\dot{F}_i(t_n)(\gamma\Delta t-(1-e^{-\gamma\Delta t})) \\
&+ (m_i)^{-1}e^{-\gamma\Delta t}\int_{t_n}^{t} e^{-\gamma(t'-t_n)}B_i(t')dt'
\end{aligned}
\qquad [49]
$$

where $\Delta t = t_{n+1} - t_n$ is the integration time-step. Note that the fluctuating force $B_i(t)$ is retained inside the integral. The ion's position is calculated with the expression,

$$
\begin{aligned}
x_i(t_{n+1}) = 2x_i(t_n) - x_i(t_{n-1})e^{-\gamma\Delta t} \\
+ \int_{t_n}^{t_n+\Delta t} v_i(t')dt' + e^{-\gamma\Delta t}\int_{t_n-\Delta t}^{t_n} v_i(t')dt'
\end{aligned}
\qquad [50]
$$

and, finally, the updated particle position is written as,

$$
\begin{aligned}
x_i(t_{n+1}) = x_i(t_n)[1+e^{-\gamma\Delta t}] - x_i(t_{n-1})e^{-\gamma\Delta t} \\
+ (m_i\gamma)^{-1}F_i(t_n)(\Delta t)[1-e^{-\gamma\Delta t}] \\
+ (m_i\gamma^2)^{-1}\dot{F}_i(t_n)(\Delta t)[0.5\gamma\Delta t(1+e^{-\gamma\Delta t})] \\
- [1-e^{-\gamma\Delta t}] + X_i^n(0,\Delta t) + e^{-\gamma\Delta t}]X_i^n(0,-\Delta t)
\end{aligned}
\qquad [51]
$$

where,

$$
X_i^n(0,\Delta t) = (m_i\gamma)^{-1}\int_{t_n}^{t_n+\Delta t}[1-e^{-\gamma(t_n+\Delta t-t')}]B_i(t')dt' \qquad [52]
$$

Equation 52 is also a Markovian stochastic process with zero mean and variance Δt. The quantity $X_i^n(0,-\Delta t)$ is correlated with $X_i^{n-1}(0,\Delta t)$ through a bivariate Gaussian distribution. In the zero-limit of the friction coefficient, this set of equations corresponds to the trajectories obtained with the Verlet algorithm [141].

The set of trajectories resulting from the Verlet-like integration scheme as compared to the Euler scheme is not limited by the velocity relaxation time, and consequently a longer time-step can be used. Figure 13 shows a plot of the steady-state average ionic energy versus time-step interval for a 150 mM KCl solution simulated for 1 ns in the absence of an external electric field. The Euler and Verlet-like algorithms give similar results for time-steps below approximately 10 fs, but larger time-steps result in a greater energy drift for the Euler integration scheme.

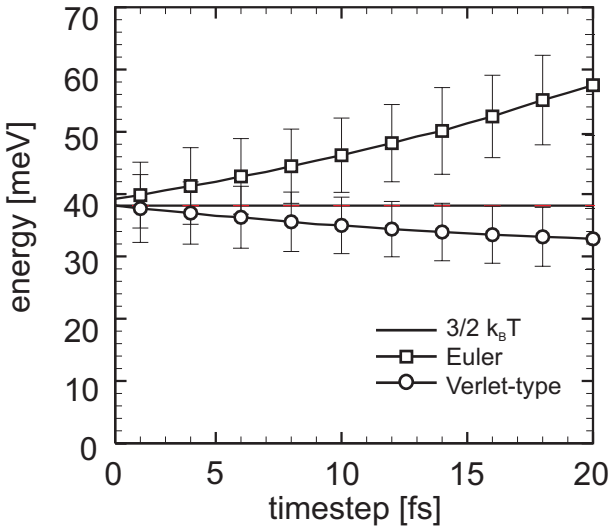

Figure 13: Steady-state energy of an ensemble of anions and cations in a 150 mM solution of KCl as a function of time-step, for both the Euler and Verlet-like integration schemes.

3.2 Explicit Solvent: Molecular Dynamics

The molecular dynamics approach allows for the simulation of the system components *individually* with atomic resolution. Broadly speaking, an appropriately constrained Newtonian dynamics is used to capture the evolution of particles representing individual ions, atoms or groups of atoms in the force field gen-

erated by electrostatic and van der Waals interactions together with boundary conditions. One difference between molecular dynamics and Brownian dynamics is the way the solvent is modeled: water molecules are typically treated explicitly within the molecular dynamics framework.

The role of water in ion permeation through narrow channels was stressed previously; a model that accounts for the dynamics of the ionic solvation state is needed for a full understanding of channel functionality. Furthermore, the atomic resolution of molecular dynamics includes sufficient information to (in principle) treat polarization effects with highly accurate, microscopic resolution. This is definitely an advantage of molecular dynamics over Brownian dynamics, which tracks the individual ionic trajectories on the atomic scale, but uses blurred-out collective properties such as the dielectric constant or the friction coefficient to express the interaction of the ions with their environment. Unfortunately, the computational burden associated with molecular dynamics simulations of ion channels is such that only relatively small systems can be simulated for times that are too short to produce statistically relevant estimates of macroscopic observables such as the ionic current flowing through an open channel [11, 143]. While it is obvious that the macroscopic parameters "friction coefficient" and dielectric coefficient will not capture the atomic detail important for ion movement or permeation in Brownian dynamics, it is not obvious that simulations of ion channels will reproduce the bulk properties of friction or dielectric response with explicit molecular dynamics methods until the simulations are actually performed and the results compared to experiment. Calibration of equilibrium systems with atomic detail form the basis of equilibrium molecular dynamics and Monte Carlo simulations of ionic solutions [95, 96].

Many models are used to include the microscopic effects of water molecules on biological systems, and most of them are based on parameterized force field schemes that are tuned to reproduce some bulk macroscopic properties of the solvent. For a given system, the choice of a specific water model is based on the usual trade-off between accuracy and computational complexity. Furthermore, even if a particular model fits a type of data better than another–for example,

dielectric constant better than density vs. temperature–the choice of which model to use is not obvious.

Water models used in ion channel simulations must reproduce, among other things, the solvent structural properties measured by the radial distribution function (RDF), mass transport characteristics like the diffusion coefficient, and the macroscopic polarization behavior, such as the dielectric constant. These models should also account for the local interactions of the water with molecules in the protein structure. This is especially important because polarization effects may play a role in the ion permeation process. It should also be noted that the bulk ionic concentrations of biologically relevant systems are relatively low, so an usually large number of solvent molecules must be simulated to ensure the presence of a statistically relevant number of ions within the simulation domain. Indeed, ions in concentrations of 10^{-6} Molar often control biological reactions of great importance: biochemistry textbooks pay much attention to the cofactors or coenzymes that control life's metabolism. The effects of these cofactors depend heavily on concentration. Thus, simulations must be able to estimate accurately the activity (i.e., effective concentration) of such trace ions if they are important in the system being studied. Consequently, the greatest number of atoms in molecular dynamics simulations is usually those of the water molecules, adding the computational efficiency as a final stringent requirement for implementing a particular solvent model. It is difficult to calculate more than a few nanoseconds of simulation time in ion channel simulations and in fact only Crozier [144, 145], to the best of the Author's knowledge, has been able to compute ion trajectories for a microsecond.

Rigid, fixed-charge water models are widely used in molecular dynamics simulations [146]. Their popularity is due to their algorithmic simplicity and to their ability to reproduce many thermodynamic properties that match experiment. Within these models, point charges combined with empirical potentials are used to model the electrostatic interaction of the water molecule [147] with its environment. The charges are placed at specific sites within the molecular volume [147] and the effective potentials are tuned to reproduce the average

(bulk) effects of polarization.

Among these approaches, 3-, 4- and 5-site models have been implemented, with different geometric configurations. Within the simple 3-site model, the positions of 3 charges are set to the sites of the hydrogen and oxygen atoms, while the negative charge is moved from the oxygen site toward the hydrogens along the bisector of the hydrogen-oxygen-hydrogen angle [146] in the 4-site representation. For the 5-site model, discrete charges are located at the positions of the hydrogen atoms, and an additional lone pair is oriented tetrahedrally around the oxygen. The number of operations in the molecular dynamics algorithms scales with the square of the number of interaction sites, thus explaining the popularity of the 3- and 4-site water models.

The family of 3- and 4-site models include the simple point charge model (SPC), and the transferable intermolecular potential functions (TIPS). The SPC is a basic 3-site model [148] with parameters adjusted to reproduce the energy and pressure of liquid water under ambient conditions. Parameters are further optimized to fit structural properties, specifically the second peak of the RDF of the oxygen atoms. The TIPS started as a 3-site liquid-phase model that was later extended to a 4-site (TIP4P) configuration [149] to reproduce the second peak structure [149] of the oxygen RDF. The TIPS and SPC based models are considered to be the most efficient since they require the lowest number of interaction calculations while providing accurate estimates of the intermolecular energy and density [144]. An extended version of the SPC fixed-charge water model was developed, which included the polarization through a mean-field description of the induced moments (SPC/E [150]). This model provides a more accurate RDF and an improvement in the calculated diffusion coefficient as compared to the standard SPC model. The parameters used in this approach are still empirical, and are adjusted to fit known physical properties. The inclusion of a realistic self-consistent description of polarization in water models is currently an important research topic.

The integration schemes used for Newtonian dynamics are simpler than that employed in the Brownian dynamics simulation based on Langevin's equation

(see the section "Implicit Solvent: Brownian Dynamics"). A popular choice [11] for Newtonian molecular dynamics is the Verlet integration scheme that conserves volume in phase space and is therefore symplectic [151]. To reduce the number of computations per unit of simulated time, much work has been devoted to integration schemes with variable time resolution [152, 153]. The idea behind these multiple-timestep methods is that a lower time resolution is required for assessing the long-range components of the force field. This translates into computing the long-range forces less frequently than the short-range forces [154].

3.2.1 Calculation of Free energy

In spite of the limitations discussed above, molecular dynamics simulations supply invaluable insight into channel functionality because *1)* they allow for a microscopic analysis of the structural fluctuations of the channel-membrane system [52, 155], and *2)* they allow for a mapping of the energetics of the ion permeation process in terms of the potential of mean force [156], which represents the free energy content of the system as a function of a reaction coordinate [157]. The free energy landscape associated with ions in the proximity of a channel can then be used as input for faster and less detailed simulation tools, such as the Brownian dynamics approach [158]. Analogously, the ion diffusion coefficient within the channel can be extracted from molecular dynamics calculations [159, 160] and used with electrodiffusive continuum models (see the next section on Flux-Based Simulation).

Indeed, all the ingredients for a complete thermodynamic characterization of the system are available in molecular dynamics simulations: atomic resolution, protein flexibility, membrane fluctuations, explicit solvent, and ionic motion. Since the free energy profile controls ion conduction [161], along with nonequilibrium parameters like the diffusion coefficient, one can expect to fully understand the permeation (and selectivity) processes from it. Furthermore, because one can explore the energetics of molecular configurations in response to external stimuli, free energy calculations can in principle supply information about

gating mechanisms, or, at least, could be used to confirm hypotheses derived from indirect experimental observations.

The task of computing free energy from molecular dynamics trajectories can be difficult because of the (non)statistical relevance of the trajectories and the inaccuracy of the force field (discussed in the next section). Extracting statistically homogeneous data from raw molecular dynamics simulations of ion channels is arduous. The highly inhomogeneous charge distribution generates a rather bumpy electrostatic landscape for the ions' dynamics. Consequently, regions of the conduction path that are needed for permeation are rarely visited by ionic trajectories [143]. Fortunately, much work has been done to enhance the statistical relevance of low-occupancy regions, and several numerical techniques have emerged as being highly effective in sampling those regions. For example, the addition of an artificial restraint on the ionic trajectories artificially biases them toward more sparsely populated regions, increasing the accuracy of the free energy profile. The effects of this external perturbing potential are then processed out of the calculated results, giving a statistically enhanced free energy profile. This technique, called umbrella sampling [162], can be used simultaneously on different regions of the same reaction coordinate, or on a multidimensional reaction space (see chapter 9 in Becker *et al.* [163]). This allows one to obtain an accurate free energy profile by means of loosely coupled simulations that can be run concurrently on separate computers. Umbrella sampling has been used to study the multi-ion free energy profile of the selectivity channel of KcsA [156], where the existence of binding sites on the extracellular side of the channel were predicted. These predictions were subsequently confirmed by high definition experimental observations [41].

3.2.2 The force field

If the ionic trajectories can be statistically enhanced by using appropriate computational techniques like umbrella sampling, it is imperative that we also increase the accuracy of the forces being computed in particle-based simulations.

State-of-the-art simulation packages use the force field decomposition discussed early in the section on electrostatics (see Eq. 1), where either the long range component of the force is neglected, or is included in the Ewald approach. Therefore, most of the simulations including long range electrostatic interactions are performed with periodic boundary conditions that bypass the problem of injecting and expelling ions and water molecules into and out of the computational domain. As stressed before, periodic boundary conditions involve several limitations that are particularly serious for ion channel simulations. For example, electrostatic boundary conditions can be applied by acting on the electric field rather than on the electrostatic potential (which is unphysically discontinuous, when not null, at the periodic boundary). This does not constitute a problem from a theoretical standpoint, but implies a representation of the simulated system that differs from reality, where potentials are applied across the system by using reversible electrodes. These limitations can be addressed by solving Poisson's equation in real space [11] and by devising an appropriate injection/ejection mechanism that mimics the effects of distant electrodes on the small domain being simulated [164].

Calculating the short-range component of the force field is crucial for an accurate particle-based simulation of ion channels. It is not possible to fully understand the permeation mechanism, especially in narrow channels, without a correct representation of the short-range interactions between the ions and the protein. The need for an accurate representation of short-range interactions is evident in KcsA, where *1)* the solvation state of the ions changes during their transit through the channel, and *2)* the narrow part of the channel (the selectivity filter) that is lined by backbone carbonyl oxygens, is being traversed by a single line of ions alternating with water molecules. The effective process of selecting and moving ions through such a narrow lumen is the result of competing microscopic interactions [155, 138] that must be accounted for precisely. The main problem is related to the force field parameters used to compute the short range components, as, for example in the Lennard-Jones potential or in the inverse power relations, as well as the other contributions like bond length-

ening, angular deformations, bond rotational barriers, etc. that are included in the potential energy functions used to describe the molecules under study. Force field parametrization is usually performed in a way that accounts for the average effects of the atomic polarization field, and involves a redistribution of the electric charge. In other words, the simulated particles (ions and atoms or groups of atoms in the protein and in the membrane) are assigned *effective* properties such as charge, size, and hardness, which normally depend on their position within the system. These force field parameters [165] are optimized in such a way that the simulation reproduces some of the desired bulk properties of the solution. The idea of the parameterization is to include the effects of the true many-body polar interactions in a simple pairwise additive fashion, so that the many-body effects can be embedded implicitly in the equations for the short range force. This approach is efficient from a computational viewpoint, but it involves a few problems. First the parametrization is not unique [138]. Second, the effects of the real polarization fields are assumed to be fixed rather than consistently evolving with the charge distribution. Finally, the effects of polarization on the molecular flexibility are necessarily neglected. It is safe to assume that in narrow pores the polarization field plays some role in the structural properties of the protein, and plays a crucial role in the ion-water and ion-protein interactions. One can try to address the problem by treating the polarization field macroscopically, *i.e.* by computing an effective position-dependent dielectric tensor at equilibrium [143], and then use this dielectric tensor in Brownian dynamics or in an appropriately modified parametrization of molecular dynamics. This approach, however, neglects the transient dynamics of the polarization fields that may assist permeation and selectivity in ultra-narrow channels.

The induced point dipole (PD) model and the fluctuating charge (FQ) model are two approaches used to include polarization explicitly in a self-consistent fashion in molecular dynamics simulations [166, 167]. Both methods define the total interaction potential as a sum of pairwise interactions (of all fixed and mobile charges) and an additional polarization term based on the induced electrostatic moments. Within the PD approach, the polarization term is included

by "inducing" a point dipole at appropriate charge sites. This dipole depends on all the other charges and all the other dipoles in the system. Therefore, the total dipole distribution must be computed as a collective (*i.e.* many-body) property of the system. This can be achieved by an iterative procedure that minimizes the polarization energy [166], or, by treating each dipole as a dynamic variable governed by a set of equations of motion. The PSPC (polarizable-SPC) model is based on this extended Lagrangian formalism, as an example.

With the FQ approach the polarization term can also be included in the model by changing the amplitude of the charges in response to the electric field. Here, a Lagrangian method is also applied to solve the set of equations of motion describing the charge dynamics. In this case, the equations are derived for the fluctuating charge system using an electronegativity equalization scheme [166]. In terms of computational resources, the FQ approach is only slightly more demanding than are the nonpolarized charge models, making it very attractive. The polarized version of the TIP4P model (TIP4P-FQ) produces RDFs that are in excellent agreement with experimental values [166].

Molecular dynamics simulations of ionic motion in hydrated ion channels have been performed for more than two decades [15, 168, 169]. Much work has been done to include explicit polarizability in molecular dynamics simulations [166, 167, 170, 171, 172] and to obtain models of water[146, 173, 174, 175, 147] that can account precisely for the local solvation properties of ions and ion channels[16, 148, 176]. A more detailed discussion of these approaches cannot be included in this document for reasons of space, so the reader is referred to the references indicated above.

4 Flux-Based Simulation

It should be clear by now that a microscopic representation of the system components can provide invaluable information for the molecular modeler that relates the structure of ion channels to their function. A major problem with such microscopic, atomistic, particle-based approaches is the inability to perform

large-scale simulation in time and space. Even optimistic guesses about the evolution of computer hardware and software place the time frame for modeling all the components of a realistically large system, of, say, a few cubic microns and for a few milliseconds, to be decades from now.

Because we want to predict and explain the complex physiological behavior of ion channels on a large scale, one can argue that all the information obtained with particle-based approaches is not actually needed. The very same issue arose more than a decade ago when algorithms were ranked for their ability to simulate semiconductor devices. State-of-the-art simulation of an individual transistor still takes hours of CPU time for picoseconds of simulated time, while key mechanisms like the trap-assisted recombination of charge carriers in the floating body of a silicon on insulator MOSFET have characteristic times of the order of hundreds of microseconds. Furthermore, even if the full characterization of an individual device could be achieved in a reasonable time, what about simulating a whole circuit where thousands of such devices are non linearly coupled? Algorithmic efficiency together with faster computing machines are not realistic solutions to such massive and complex problems.

It is our opinion (and probably the most important message that we try to convey in this chapter) that any approach for simulating complex, many-body systems must be based on a hierarchy of consistently related models (see the next section below). Each model employed must be validated individually by comparison (direct or indirect) with experimental data, and, the range of validity for each model must be defined as clearly as possible. Knowing in which cases we can safely apply a theory then makes that theory practical.

With this background we devote this section to approaches based on continuum ionic charge distributions rather than limiting this tutorial to the discussion of particle-based simulation methods. These electrodiffusive approaches are called here flux-based because they model the flux of charges, *i.e.*, the current densities, flowing through the system. Electrostatic and van der Waals interactions are accounted for implicitly by a mean field approach where their effects are included as averages over the many instantaneous configurations that the

particle-based approaches would otherwise model individually. The main assumption made with the flux-based approaches is therefore that the ion channel behavior can be explained by their mean structural properties rather than by the instantaneous microscopic dynamics of the system.

4.1 Nernst-Planck Equation

One continuum model for electrodiffusion of ions between regions of different concentration is based upon the combination of Fick's law [177] that describes the diffusion of ions along a concentration gradient and Kohlrausch's law that describes the drift of ions along a potential gradient. Nernst and Planck combined these two laws to obtain the electrodiffusive equation, now known as the Nernst-Planck equation, and which can be written in the Stratonovich form [178, 179] as,

$$\frac{d}{d\vec{r}}\left\{D(\vec{r})\left[\nabla c(\vec{r}) + \frac{q}{k_B T}\nabla\Phi(\vec{r})c(\vec{r})\right]\right\} = 0 \qquad [53]$$

Here D is the diffusion coefficient, c is the ionic concentration, and Φ is the electrostatic potential due to the charges within the system and the external boundary conditions. The absolute temperature of the solution is T, while k_B is Boltzmann's constant and q is the ionic charge. Integrating Eq. 53 once, gives,

$$D(\vec{r})\left[\nabla c(\vec{r}) - \frac{1}{k_B T}\vec{F}(\vec{r})c(\vec{r})\right] = -\vec{J} \qquad [54]$$

where $\vec{J}$ is the constant steady-state current density vector, and $\vec{F}(\vec{r})$ is the force as calculated through the gradient of the electrostatic potential. Both the concentration c and the force field $\vec{F}$ are space-dependent unknowns in the problem, so two additional equations are coupled to Eq. 54 to obtain $\vec{J}$: the continuity equation,

$$\frac{1}{q}\nabla\cdot\vec{J} = -\frac{\partial c}{\partial t} + G \qquad [55]$$

and Poisson's equation (Eq. 18). The quantity G in Eq. 55 represents the mech-

anisms of charge generation and recombination occurring within the system. In the following discussion it is assumed to be null for the sake of simplicity. For an one-dimensional domain starting at $x = 0$ and ending at $x = L$, the solution to Eq. 54 can be written as [180]:

$$\vec{J} = \frac{c(0)e^{\Phi(0)/k_BT} - c(L)e^{\Phi(L)/k_BT}}{\int_0^L e^{\Phi(x)/k_BT}\frac{dx}{D(x)}} \qquad [56]$$

The set of three coupled equations (Eq. 18, Eq. 54, and Eq. 55) is then solved numerically with an iterative procedure that will be discussed in a subsequent section.

The remainder of this section is devoted to the derivation of Eq. 54. Besides the mathematics we also define the range of applicability of simulations based on the Nernst-Planck equation. The starting point for deriving the Nernst-Planck equation is Langevin's equation (Eq. 45). A solution of this stochastic differential equation can be obtained by finding the probability that the solution in phase space is $\vec{r}, \vec{v}$ at time t, starting from an initial condition $\vec{r}_0, \vec{v}_0$ at time $t = 0$. This probability is described by the probability density function $p(\vec{r}, \vec{v}, t)$. The basic idea is to find the phase-space probability density function that is a solution to the appropriate partial differential equation, rather than to track the individual Brownian trajectories in phase space. This last point is important, because it defines the difference between particle-based and flux-based simulation strategies.

The derivation of a differential equation for $p(\vec{r}, \vec{v}, t)$ is performed by first defining the diffusion process as an independent Markov process in order to write a Chapman-Kolmogorov equation in phase space:

$$p(\vec{r} + \vec{v}\Delta t, \vec{v}, t + \Delta t) = \int p(\vec{r}, \vec{v} - \Delta\vec{v}, \Delta t)\Psi(\vec{r}, \vec{v} - \Delta\vec{v}; \Delta\vec{v})d(\Delta\vec{v}) \qquad [57]$$

In Eq. 57 Δt is a time interval chosen to satisfy two criteria: *1)* during Δt the position and velocity do not change appreciably, and *2)* the stochastic term in

Langevin's equation must undergo many fluctuations. Equation 57 states the Markovian nature of $p(\vec{r}, \vec{v}, t)$.

Applying a Taylor expansion to each of the individual terms in Eq. 57 results in the generalization of the Fokker-Planck equation [181] for the evolution of $p(\vec{r}, \vec{v}, t)$ in phase-space:

$$\frac{\partial p}{\partial t} + \vec{v} \cdot \nabla_r p + \frac{\vec{F}}{m} \cdot \nabla_v p = \gamma \nabla_v \cdot (p\vec{v}) + \gamma \frac{k_B T}{m} \nabla_v^2 p \qquad [58]$$

It should be noted that the left-hand side of Eq. 58 is identical to that of the reduced Liouville equation [181]. Indeed, several theories have been developed that obtain Eq. 58 from the reduced Liouville equation [182, 181]. Following the standard Smoluchowski expansion [178] of the full time-dependent Fokker-Planck equation, it can be shown that, for large γ, the following model is obtained for the probability density at steady state:

$$\frac{d}{d\vec{r}} \left\{ \frac{1}{\gamma} \left[\frac{k_B T}{m} \nabla p(\vec{r}) + \frac{q}{m} \nabla \Phi(\vec{r}) p(\vec{r}) \right] \right\} = 0 \qquad [59]$$

Note that the dependence of p on the velocity has been dropped because of the overdamping hypothesis (*i.e.* large γ), and $p(\vec{r}) \equiv \lim_{t \to \infty} p(\vec{r}, t)$ which is a consequence of the steady state hypothesis. Equation 59 is clearly written in the Stratonovich form (see Eq. 53).

The probability distribution functions in Eq. 59 applied to the trajectories of particles flowing into and out of a system provides a justification for using the Nernst-Planck equation (Eq. 54): the net ionic directional fluxes can be expressed in terms of differences between the probability fluxes, normalized to the concentration at the sides of the region of interest [180]. That ionic fluxes and differences in probability fluxes are related thus supplies a connection between the solution of the Nernst-Planck equation (Eq. 54) and the Smoluchowski equation (Eq. 59), and provides a direct justification for using Eq. 54 for the study of ions subjected to Brownian dynamics in solution.

Continuing along these lines, we also observe that the Liouville equation is used to obtain the Boltzmann transport equation derived initially within the

kinetic theory of gases:

$$\frac{\partial f}{\partial t} + \vec{v} \cdot \nabla_r f + \frac{\vec{F}}{m} \cdot \nabla_v f = \left(\frac{\partial f}{\partial t} \right)_{coll} \quad [60]$$

where $f(\vec{r}, \vec{v}, t)$ is the phase-space point density, or distribution function, of the particles. The right hand term of Eq. 60 represents the time rate of change of $f(\vec{r}, \vec{v}, t)$ due to collisions that particles undergo within the system.

We now conclude with a derivation of the basic transport equations starting from the Boltzmann equation rather than from the Fokker-Planck equation. We already noted that both the Fokker-Planck and Boltzmann equations are related to the Liouville equation and that our goal is to obtain equations for the charge distribution and the current density (Eqs. 55 and 54) using an appropriate representation of the collisional term in the left hand side of Eq. 60. The method described here is the well known methods of moments. It consists of multiplying the Boltzmann equation by a power of the velocity, and by integrating over the velocity itself. For the moment of order zero (i.e., the zeroth power of the velocity), one uses a constant; that, in this case is the elemental charge q, to obtain

$$\frac{1}{q} \nabla \cdot (qc\vec{v}) = -\frac{\partial c}{\partial t} + G \quad [61]$$

where G is the integral of the collisional term:

$$G = -\int \left(\frac{df}{dt} \right)_{coll} d\vec{v} \quad [62]$$

Based on the assumption that collisions change the ionic velocity but not their position, G is simply reduced to a charge generation-recombination term that will be neglected in processes involving transport. By recalling that $\vec{J} = qc\vec{v}$, one realizes that Eq. 61 is the continuity equation previously written (see Eq. 55).

The moment of order one is obtained by multiplying the Boltzmann equation by $\vec{v}$ and integrating over the velocity space. The result is given by:

$$\frac{\partial}{\partial t}(c\vec{v}) + \vec{v}\nabla_r \cdot (c\vec{v}) + (c\vec{v} \cdot \nabla_r)\vec{v} + \frac{1}{m}\nabla_r \cdot (ck_B\hat{T}) + \frac{\vec{F}}{m}c = \left(\frac{\partial \vec{v}}{\partial t}\right)_{coll} \quad [63]$$

where $\hat{T}$ is the temperature tensor. Equation 63 is simplified considerably by assuming that the concentration c is not a function of time (steady-state assumption). This is accomplished by neglecting the convection term $\vec{v}\nabla \cdot (c\vec{v})$, by representing the tensor $\hat{T}$ with the scalar T, and, finally, by assuming that the evolution of the velocity is a sequence of stationary states. Furthermore, assuming that the fluctuations of the velocity generate small deviations from equilibrium, one can apply a relaxation time approximation [183] to the collisional term,

$$\left(\frac{\partial \vec{v}}{\partial t}\right)_{coll} \approx \vec{v}\gamma \quad [64]$$

These assumptions allow us to write Eq. 63 as

$$D(\vec{r})\left[\nabla c(\vec{r}) - \frac{1}{k_B T}\vec{F}(\vec{r})c(\vec{r})\right] = -\vec{J} \quad [65]$$

which is the Nernst-Planck equation, where the diffusion coefficient is expressed as $D = \frac{k_B T}{\gamma}$.

Because Boltzmann's equation is a conservation relation in phase space, its moments represent conservation laws in position space $\vec{r}$. In particular, the moment of order zero, Eq. 61, is the charge conservation law, while Eq. 65 represent current conservation. The next moment is obtained by multiplying Eq. 60 by $mv^2/2$ and integrating over the velocity space. The resulting equation is an energy conservation relation that accounts for heat flow within the system. Inspired by the literature on semiconductor modeling and simulation [184], Chen solved the system for the first three moments of Boltzmann's equation within the ion channel framework [185], proposing the inclusion of kinetic energy exchange between the different components of the system.

4.2 The PNP Method

This section describes the numerical techniques used for solving the set of differential equations that are used to model the electrodiffusion of ions in solution. The method has historically been called the Poisson-Nernst-Planck (PNP) method because it is based on the coupling of the Poisson equation with the Nernst-Planck equation. The basic equations used in the PNP method include the Poisson equation (Eq. 18), the charge continuity equation (Eq. 55) and the current density of Nernst-Planck equation (Eq. 54).

Poisson's equation is usually simplified by assuming the dielectric constant to be stepwise constant in the position space. It should be noted that this approximation does not preclude the possibility of having dielectric interfaces within the computational domain, what is assumed here is that the dielectric constant changes abruptly at the interface of different materials. This assumption is completely natural when Poisson's equation is solved on a discrete grid by a finite differences scheme.

Equations 18, 54, and 55 constitute a system of three equations with three unknowns, and is solved numerically on 1-, 2- or 3D domains. For the sake of simplicity, we will discuss the one-dimensional case (the equations are easily extended to 3D). While finite element methods have been used extensively for the solution of Eqs. 18, and 55 in solid state electronics, flux-based approaches for the simulation of ion channels rely primarily on finite difference schemes.

The system of Eqs. 18, 54, and 55 is usually solved iteratively, with each iteration defined by the successive solution of the three equations. An initial guess is first supplied for the force field $\vec{F}$ in Eq. 54, that is then solved on a discrete grid to provide the components of the current density $\vec{J}$. The divergence of $\vec{J}$ is then computed with the steady-state continuity equation (Eq. 55) to obtain the charge distribution that, in turn, is used in the forcing function of Poisson's equation. From the gradient of the computed potential one derives a new (better) approximation to the force $\vec{F}$ that is used to start another iteration. The iterative process is repeated until the difference between the results of two

successive iterations reaches a predefined threshold value. This process ensures self-consistency between the spatial distributions of the charge, current, and potential.

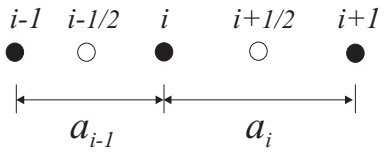

Figure 14: Discretization scheme used for the solution of the PNP equations. Values of the current density are computed at the points designated by empty circles, the potential and charge density values are computed at points corresponding to the filled circles.

The numerical method for solving of the PNP system is normally based on the discretization scheme in Fig. 14. A grid is initially defined upon which the values of potential and charge distributions are computed (filled circles in Fig. 14), while the components of the current density vector are computed on points located half way between those grid-points (empty circles). Because methods for solving Poisson's equation were already discussed, the remaining part of this discussion will focus on the solution of the continuity equation. For a discretization scheme as in Fig. 14, one can write a first order finite difference equation for the continuity equation:

$$\frac{\partial c}{\partial t} = \frac{1}{q}\nabla \cdot \vec{J} = \frac{1}{q}\left[\frac{J_{i+1/2} - J_{i-1/2}}{\frac{a_i + a_{i-1}}{2}}\right] = 0 \qquad [66]$$

where $J_{i+1/2} = J_x(x_{i+1/2})$, a represents the mesh spacing, and the system is assumed to be in steady-state. The values of the current can be obtained by finite difference equations obtained from Eq. 54:

$$J_{i+1/2} = D_{i+1/2}\frac{c_{i+1} - c_i}{a_i} - c_{i+1/2}\frac{D_{i+1/2}}{k_B T}F_{i+1/2} \quad [67a]$$

$$J_{i-1/2} = D_{i-1/2}\frac{c_i - c_{i-1}}{a_{i-1}} - c_{i-1/2}\frac{D_{i-1/2}}{k_B T}F_{i-1/2} \quad [67b]$$

where the values of any function at the midpoint locations (empty points in Fig. 14) are obtained through linear interpolation. The currents from Eqs. 67a and 67b can then be used in Eq. 66 to obtain a difference equation that expresses the concentration c as a function of the force F. In 2- and 3D domains, the difference equations are normally solved by using a standard iterative method.

This solution scheme for the PNP method is attractive for its simplicity, but, it leads to substantial errors in those regions where there exists large concentration gradients. Within this approach, the lack of robustness is traced to the assumption that the ion concentration varies linearly between adjacent grid cells (see Eqs. 67). The discretization of the gradient operator in the current density equation results in negative values for the concentration when the difference of potential between adjacent cells exceeds $2k_BT/q$ volts [186]. An effective solution to this problem has been suggested by Sharfetter and Gummel [187, 188] who demonstrated that the discretization errors can be substantially reduced by including a nonlinear exponential variation of ion concentration between grid points. In this case, Eqs. 67a and 67b are rewritten as,

$$J_{i+1/2} = -qF_{i+1/2}\left[\frac{\frac{D_{i+1/2}}{k_B T}\ c_{i+1}}{1 - \exp[\frac{F_{1+1/2}}{q}a_i]} + \frac{\frac{D_{i+1/2}}{k_B T}\ c_i}{1 - \exp[\frac{-F_{1+1/2}}{q}a_i]}\right] \quad [68a]$$

$$J_{i-1/2} = -qF_{i-1/2}\left[\frac{\frac{D_{i-1/2}}{k_B T}\ c_i}{1 - \exp[\frac{F_{1-1/2}}{q}a_{i-1}]} + \frac{\frac{D_{i-1/2}}{k_B T}\ c_{i-1}}{1 - \exp[\frac{-F_{1-1/2}}{q}a_{i-1}]}\right] \quad [68b]$$

Again, the current from Eqs. 68a and 68b can be used to obtain a difference scheme for the concentration via the continuity equation. The method of Sharfetter and Gummel is slightly slower than the linearized approach, but, it is more

accurate and is remarkably more robust in the presence of high concentration gradients. Furthermore, it produces positive definite matrices and hence can be implemented by using overrelaxation techniques [119], which have a relatively fast rate of convergence. Multi–grid methods [125] have also been used successfully for solving PNP-like equations (see Molenaar [189] and references therein). Finally, it should be noted that the approach suggested by Eisenberg [180] (which is also based on the iterative solution of the continuity equation, the analytical solution of the Nernst-Planck equation (Eq. 56), and Poisson's equation (Eq. 18)) is mathematically equivalent to the Gummel iteration once it has been discretized on a finite difference grid.

The evolution of the numerical approaches used for solving the PNP equations has paralleled the evolution of computing hardware. The numerical solution to the PNP equations evolved over the time period of a couple of decades beginning with the simulation of extremely simplified structures [84, 190] to fully 3D models [22, 191, 192], and with the implementation of sophisticated variants of the algorithmic schemes to increase robustness and performance [20]. Even finite element tetrahedral discretization schemes have been employed successfully to selectively increase the resolution in regions inside the channels [21]. An important aspect of the numerical procedures being described above is the need for full self-consistency between the force field and the charge distribution in space. This is obtained by coupling a Poisson solver to the Nernst-Planck solver [1, 193] within the iteration scheme described above.

The PNP approach, together with the Poisson-Boltzmann [194, 195] method, belong to the family of continuum theories of electrolytes [196] that are based on the mean field approximation. Because the PNP approach is based on continuous fluxes rather than individual trajectories, average concentrations are employed and the ions are assumed to move in average electric fields [1]. Consequently, a key role is played by *macroscopic* parameters such as the diffusion coefficient and the dielectric constant. Recall that the term macroscopic is being used to represents the *collective* behavior of a large group of microscopic components of the system, *i.e.*, atoms within molecules and ions in solution.

While the PNP theory has been developed as a model for large systems, *e.g.* those with feature-sizes larger than the Debye length, its applicability in modeling ionic permeation within channels only a few angstroms across has been questioned [197, 198]. Similar concerns have been expressed with respect to the Poisson-Boltzmann method [199]. It should be noted, however, that the relevant Debye length in either method is that within the channel (or active site) and not that in bulk. The concentration of ions is typically 10-50 times higher inside a channel than in bulk, and consequently the Debye length is extremely small there.

From a physical viewpoint, the use of a fixed diffusion coefficient corresponds to assuming that the ionic energy relaxation time is independent of the local electric field. The same approximation is applicable to the friction coefficient γ in Langevin's equation. Generally speaking, ion channels are not ohmic machines, at not least during the transient conditions typical of gating. Because of the steady-state assumption, the PNP method is not suitable for the study of fast transients or situations in which the ionic energy is different from the energy of the surrounding system. Nonetheless, because it can supply valuable information for the study of the steady-state ohmic regime, assuming a constant diffusivity has been a popular choice by scientists studying ion channels. Alternatively, and similarly to what is done for the simulation of semiconductor devices, a space-dependent diffusivity for a specific channel configuration can be obtained with particle-based simulation (usually molecular dynamics) and used in the PNP equations [160].

Solving the PNP equations is more complicated when including the effects of polarization. Defining a dielectric "constant" within a small channel presents huge conceptual difficulties. From a microscopic viewpoint, the dynamics of one ion (or more) within the channel is being described as a purely many-body problem, meaning that the presence of even one ion modifies significantly the polarization field felt by the ion itself, and, possibly, even the structural conformation of the channel protein. It is reasonable to conclude that the polarization plays a role in the conduction properties (including selectivity) of very nar-

row channels and possibly even wider channels. The interaction of ions with dielectric surfaces is definitely a local phenomenon related to the particle character of the ions themselves. However, continuum theories represent ions as a smooth charge distribution rather than as point-like charges, and modeling effects of the dielectric interfaces on such distributed charge is thus particularly arduous. A typical example is the problem of "overshielding" shown by PNP simulations of narrow channels. The continuous nature of PNP results in the formation of a spurious counter-charge in the channel that is already populated by a given ionic species. This flow of counter-charge represents counter-ions that would not normally enter the channel because of their interaction with the image charges generated at the channel dielectric surface. This spurious and non-realistic effect, in contrast, is not produced by particle-based Brownian dynamics simulations because the finite size of ions is included in Brownian dynamics. The spurious counter-charge modifies the electrostatic landscape, and consequently a remarkable discrepancy is found in the ionic concentrations when comparing results obtained with Brownian dynamics [198]. Several adjustments to the PNP theory have been proposed to alleviate this problem, either via the inclusion of a term that accounts for the induced image charges as a surface charge in Poisson's equation [200], or, by correcting the free energy of the system with a potential of mean force [181] obtained from molecular dynamics simulations [160]. These extended theories offer better agreement with results from particle-based approaches [201], at least for single channel occupancy and in very narrow channels.

In conclusion, flux-based approaches are appealing because of their low computational costs and because of their ability to predict quantities that are directly observable, such as currents flowing through open channels. Their utility for the study of small channels has been questioned, especially because of the argued inability to account for molecular flexibility. Therefore, much theoretical work is needed to extend and generalize the flux-based simulation approaches to better account for more realistic configurations, keeping in mind their basic limitations. Several researchers rightly stressed the need for validating flux-based

simulation with microscopic particle-based models. Analogously, particle-based models must also be validated on the largest scales for which they are used, in the hierarchy of models (see below).

5 Hierarchical Simulation Schemes

Several approaches for the simulation of ionic charge transport in protein channels have been presented in the previous sections. It should be clear from the above discussion that none of the mentioned methods can supply a complete and self-contained description of the full functionality of ion channels starting from purely structural information. For this reason, methods based on a hierarchy of simulative approaches [202, 203], rather than on a specific method are becoming more and more popular.

The concept of using atomistic molecular dynamics simulations for extracting parameters to be used in less precise but faster Brownian dynamics simulators, or electrodiffusive solvers, has been discussed above. This methodology can be applied rather extensively, and can entail molecular mechanics techniques for the full preparation of the protein structure, continuum techniques for its electrostatic characterization, and molecular dynamics for the extraction of diffusion or energy profiles for use in Brownian dynamics [204]. This "sequential" approach has been used with excellent results in other fields, and is well established in computational biophysics [205]. A further step in the direction of hierarchical modeling is to use different approaches simultaneously, and to analyze the (sometimes different) results by keeping in mind strengths and weaknesses of the simulative methodologies. This "parallel" or comparative strategy has a certain degree of subjectivity that can be minimized if a rigorous attitude is adopted by the modeler throughout the study when interpreting the results [51], and by calibrating the methods.

Furthermore, due to the limitations in the size of the systems that can be simulated with high resolution, all-atom techniques, the integration of different approaches into the same simulation procedure is necessary in the foreseeable

future. For example, using a molecular dynamics simulation engine in a relatively small region of the system under study and including a larger domain where the solvent can be treated implicitly, say with Brownian dynamics, will allow for extending the size of the simulated system and to reduce artifacts arising from close boundaries. Of course, the correct treatment of the interface that "bridges" two regions simulated with different computational and philosophical approaches is not trivial and solving such problems has not yet been accomplished.

6 Future Directions and Concluding Remarks

The recent development of high resolution experimental techniques allows for the structural analysis of protein channels with unprecedented detail. However, the fundamental problem of relating the structure of ion channels to their function is a formidable task. This chapter describes some of the most popular simulation approaches used to model channel systems. Particle-based approaches such as Brownian and molecular dynamics will continue to play a major role in the study of protein channels and in validating the results obtained with the extremely fast continuum models. Research in the area of atomistic simulations will focus mainly on the force-field schemes used in the ionic dynamics simulation engines. In particular, polar interactions between the various components of the system need to be computed with algorithms that are more accurate than those currently used. The effects of the local polarization fields need to be accounted for explicitly and, at the same time, efficiently. Continuum models will remain attractive for their efficiency in depicting the electrostatic landscape of protein channels. Both Poisson-Boltzmann and Poisson-Nernst-Plank solvers will continue to be used to extract qualitative information about the macroscopic behavior of ion channels. Their quantitative predictions will become better valued once the range of applicability of the theory is validated by particle-based approaches. These improvements will help scientists address how the functional properties of ion channels depend on the instantaneous structural fluctuations

and to what extent a mean conformational characteristic is sufficient to describe these amazingly complex systems.

The idea of integrating different approaches into a hierarchical simulation strategy is promising. This can be accomplished either through a "sequential" approach, in which the results obtained with one method are used to calibrate a faster but less accurate one, or though a "concurrent" technique, in which several simulation tools are integrated or "bridged" within the same algorithm in a way that provides different levels of accuracy in different regions of the computational domain.

References

[1] B. Hille, *Ionic Channels of Excitables Membranes*, Sinauer, Massachusetts, 3^{rd} ed., 2001.

[2] E. Neher and B. Sackmann, *Nature*, **260**, 799 (1976). Single-Channel Currents Recorded from Membrane of Denervated Frog Muscle Fibers.

[3] B. Sakmann and E. Neher, Eds., *Single-Channel Recording*, Kluwer Academic, 2^{nd} ed., 1995.

[4] F. Ashcroft, *Ion Channels and Disease*, Academic Press, San Diego, 2000.

[5] L.-Q. Gu, O. Braha, S. Conlan, S. Cheley, and H. Bayley, *Nature*, **398**, 686 (1999). Stochastic Sensing of Organic Analytes by a Pore-forming Protein Containing a Molecular Adapter.

[6] H. Bayley and P. Cremer, *Nature*, **413**, 226 (2001). Stochastic Sensors Inspired by Biology.

[7] M. Goryll, S. Wilk, G. M. Laws, T. Thornton, S. Goodnick, M. Saraniti, J. Tang, and R. S. Eisenberg, *Superlattices Microstruct. (*in press) (2004). Silicon-based Ion Channel Sensor.

[8] S. Sze, *Physics of Semiconductor Devices*, John Wiley & Sons, New York, 2^{nd} ed., 1981.

[9] Semiconductor Industry Association, International SEMATECH, Austin - TX, 1999; chapter Process Integration, Devices, and Structures, pp. 83–103; International Technology Roadmap for Semiconductors.

[10] E. R. Davidson, in *Reviews in Computational Chemistry*, K. B. Lipkowitz and D. B. Boyd, Eds., VHC Publishers, New York, 1990, Vol. 6, pp. 373–382. Perspectives on *Ab Initio* Calculations.

[11] H. Berendsen in *Computational Molecular Dynamics: Challenges, Methods, Ideas*, P. Deuflhard, Ed.; Springer-Verlag, 1999; pp. 3–36.

[12] P. Gibbon and G. Sutmann in *Quantum Simulations of Many-Body Systems: From Theory to Algorithms, Lecture Notes*, J. Grotendorst, D. Marx, and A. Muramatsu, Eds., Vol. 10 of *NIC;* John von Neumann Institute for Computing, Jülich, Germany, 2002; pp. 467–506.

[13] D. E. Elmore and D. A. Dougherty, *Biophys. J.*, **85**(3), 1512 (2003). Investigating Lipid Composition Effects on the Mechanosensitive Channel of Large Conductance (MscL) Using Molecular Dynamics Simulations.

[14] B. L. de Groot, D. P. Tieleman, P. Pohl, and H. Grubmuller, *Biophys. J.*, **82**(6), 2934 (2002). Water Permeation through Gramicidin A: Desformylation and the Double Helix: A Molecular Dynamics Study.

[15] W. Lee and P. Jordan, *Biophys. J.*, **46**(6), 805 (1984). Molecular Dynamics Simulation of Cation Motion in Water-Filled Gramicidin like Pores.

[16] S. Chiu, S. Subramaniam, E. Jakobsson, and J. McCammon, *Biophys. J.*, **56**(2), 253 (1989). Water and Polypeptide Conformations in the Gramicidin Channel. A Molecular Dynamics Study.

[17] B. Roux and M. Karplus, *Biophys. J.*, **59**(5), 961 (1991). Ion Transport in a Model Gramicidin Channel. Structure and Thermodynamics.

[18] J. A. Szule and R. P. Rand, *Biophys. J.*, **85**(3), 1702 (2003). The Effects of Gramicidin on the Structure of Phospholipid Assemblies.

[19] T. Allen, O. Anderson, and B. Roux, *PNAS*, **101**(1), 117 (2004). Energetics of Ion Conduction Through the Gramicidin Channel.

[20] M. G. Kurnikova, R. D. Coalson, P. Graf, and A. Nitzan, *Biophys. J.*, **76**(2), 642 (1999). A Lattice Relaxation Algorithm for Three-Dimensional Poisson-Nernst-Planck Theory with Application to Ion Transport Through the Gramicidin A Channel.

[21] U. Hollerbach, D. Chen, D. Busath, and B. Eisenberg, *Langmuir*, **16**(13), 5509 (2000). Predicting Function from Structure using the Poisson-Nernst-Plank Equations: Sodium Current in the Gramicidin A Channel.

[22] U. Hollerbach, D. Chen, and R. Eisenberg, *J. Sci. Comput.*, **16**(4), 373 (2001). Two- and Three-Dimensional Poisson-Nernst-Plank Simulations of Current Flow Through Gramicidin A.

[23] S. Edwards, B. Corry, S. Kuyucak, and S.-H. Chung, *Biophys. J.*, **83**(3), 1348 (2002). Continuum Electrostatics Fails to Describe Ion Permeation in the Gramicidin Channel.

[24] T. Allen, T. Bastug, S. Kuyucak, and S.-H. Chung, *Biophys. J.*, **84**(4), 2159 (2003). Gramicidin A Channel as a Test Ground for Molecular Dynamics Force Fields.

[25] D. Urry, *PNAS*, **68**, 672 (1971). The Gramicidin A Transmembrane Channel: A Proposed π_{LD} Helix.

[26] R. Ketchem, W. Hu, and T. Cross, *Science*, **261**, 1457 (1993). High-Resolution Conformation of Gramicidin A in a Lipid Bilayer by Solid-State NMR.

[27] L. Townsley, W. Tucker, S. Sham, and J. Hinton, *Biochemistry*, **40**, 11676 (2001). Structures of Gramicidin A, B and C Incorporated in Sodium Dodecyl Sulfate Micelles.

[28] T. W. Allen, O. S. Andersen, and B. Roux, *J. Amer. Chem. Soc.*, **125**(32), 9868 (2003). Structure of Gramicidin a in a Lipid Bilayer Environment Determined Using Molecular Dynamics Simulations and Solid-State NMR Data.

[29] Y. Chen, A. Tucker, and B. Wallace, *J. Mol. Biol.*, **264**(4), 757 (1996). Solution Structure of a Parallel Left-Handed Double-Helical Gramicidin-A Determined by 2D lH NMR.

[30] R. Ketchem, W. Hu, and T. Cross, *J. Biomol. NMR*, **8**(1), 1 (1996). Macromolecular Structure Elucidation with Solid-State NMR-Derived Orientation Constraints.

[31] T. A. Harroun, W. T. Heller, T. M. Weiss, L. Yang, and H. W. Huang, *Biophys. J.*, **76**(6), 3176 (1999). Theoretical Analysis of Hydrophobic Matching and Membrane-Mediated Interactions in Lipid Bilayers Containing Gramicidin.

[32] S.-W. Chiu, S. Subramaniam, and E. Jakobsson, *Biophys. J.*, **76**(4), 1929 (1999). Simulation Study of a Gramicidin/Lipid Bilayer System in Excess Water and Lipid. I. Structure of the Molecular Complex.

[33] T. A. Harroun, W. T. Heller, T. M. Weiss, L. Yang, and H. W. Huang, *Biophys. J.*, **76**(2), 937 (1999). Experimental Evidence for Hydrophobic Matching and Membrane-Mediated Interactions in Lipid Bilayers Containing Gramicidin.

[34] S.-W. Chiu, S. Subramaniam, and E. Jakobsson, *Biophys. J.*, **76**(4), 1939 (1999). Simulation Study of a Gramicidin/Lipid Bilayer System in Excess Water and Lipid. II. Rates and Mechanisms of Water Transport.

[35] G. V. Miloshevsky and P. C. Jordan, *Biophys. J.*, **86**(1), 92 (2004). Gating Gramicidin Channels in Lipid Bilayers: Reaction Coordinates and the Mechanism of Dissociation.

[36] K. M. Armstrong and S. Cukierman, *Biophys. J.*, **82**(3), 1329 (2002). On the Origin of Closing Flickers in Gramicidin Channels: A New Hypothesis.

[37] G. S. Harms, G. Orr, M. Montal, B. D. Thrall, S. D. Colson, and H. P. Lu, *Biophys. J.*, **85**(3), 1826 (2003). Probing Conformational Changes of Gramicidin Ion Channels by Single-Molecule Patch-Clamp Fluorescence Microscopy.

[38] D. Tieleman, P. Bigging, G. Smith, and M. Sansom, *Quarterly Reviews of Biophysics*, **34**(4), 473 (2001). Simulation Approaches to Ion Channel Strucuture-Function Relationships.

[39] W. Humphrey, A. Dalke, and K. Schulten, *J. Mol. Graphics Model.*, **14**(1), 33 (1996). VMD-Visual Molecular Dynamics.

[40] D. Doyle, J. Cabral, R. Pfuetzner, A. Kuo, J. Gulbis, S. Cohen, B. Chait, and R. MacKinnon, *Science*, **280**, 69 (1998). The Structure of the Potassium Channel: Molecular Basis of K^+ Conduction and Selectivity.

[41] Y. Zhou, J. Morales-Cabral, A. Kaufman, and R. MacKinnon, *Nature*, **414**, 43 (2001). Chemistry of Ion Coordination and Hydration Revealed by a K^+ Channel-Fab Complex at 2.0 ÅResolution.

[42] Y. Jiang, A. Lee, J. Chen, M. Cadene, B. Chait, and R. MacKinnon, *Nature*, **417**, 515 (2002). Crystal Structure and Mechanism of a Calcium-Gated Potassium Channel.

[43] G. Yellen, *Nature*, **419**, 35 (2002). The Voltage-Gated Potassium Channels and Their Relatives.

[44] Y. Jiang, A. Lee, J. Chen, V. Ruta, M. Cadene, B. Chait, and R. MacKinnon, *Nature*, **423**, 33 (2003). X-ray Structure of a Voltage-Dependent K^+ Channel.

[45] E. Perozo, D. Cortes, and L. Cuello, *Science*, **285**, 73 (1999). Structural Rearrangements Undelying K^+-Channel Activation Gating.

[46] Y. Jiang, V. Ruta, J. Chen, A. Lee, and R. MacKinnon, *Nature*, **423**, 42 (2003). The Principle of Gating Charge Movement in a Voltage-Dependent K^+ Channel.

[47] C. Ahern and R. Horn, *J. Gen. Physiol.*, **123**, 205 (2004). Specificity of Charge-Carrying Residues in the Voltage Sensor of Potassium Channels.

[48] B. Roux and R. MacKinnon, *Science*, **285**, 100 (1999). The Cavity and Pore Helices in the KcsA K^+ Channel: Electrostatic Stabilization of Monovalent Cations.

[49] E. M. Nestorovich, T. K. Rostovtseva, and S. M. Bezrukov, *Biophys. J.*, **85**(6), 3718 (2003). Residue Ionization and Ion Transport Through OmpF Channels.

[50] S. Varma and E. Jakobsson, *Biophys. J.*, **86**(2), 690 (2004). Ionization States of Residues in OmpF and Mutants: Effects of Dielectric Constant and Interactions Between Residues.

[51] W. Im and B. Roux, *J. Mol. Biol.*, **322**(4), 851 (2002). Ion Permeation and Selectivity of OmpF Porin: A Theoretical Study Based on Molecular Dynamics, Brownian Dynamics, and Continuum Electrodiffusion Theory.

[52] W. Im and B. Roux, *J. Mol. Biol.*, **319**(5), 1177 (2002). Ions and Counterions in a Biological Channel: A Molecular Dynamics Simulation of OmpF Porin from Escherichia Coli in an Explicit Membrane with 1 M KCl Aqueous Salt Solution.

[53] A. Karshikoff, V. Spassov, S. Cowan, R. Ladenstein, and T. Schirmer, *J. Mol. Biol.*, **240**, 372 (1994). Electrostatic Properties of Two Porin Channels from Escherichia Coli.

[54] A. Philippsen, W. Im, A. Engel, T. Schirmer, B. Roux, and D. Muller, *Biophys. J.*, **82**(3), 1667 (2002). Imaging the Electrostatic Potential of Transmembrane Channels: Atomic Probe Microscopy of OmpF Porin.

[55] B. Alberts, D. Bray, A. Johnson, J. Lewis, M. Raff, K. Roberts, and P. Walter, *Essential Cell Biology*, Garland Publishing, Inc, New York, 1998.

[56] K. Damodaran and K. Merz Jr., in *Reviews in Computational Chemistry*, K. B. Lipkowitz and D. B. Boyd, Eds., VHC Publishers, New York, 1994, Vol. 5, pp. 269–298. Computer Simulation of Lipid Systems.

[57] J. M. Berg, J. L. Tymoczko, and L. Stryer, *Biochemistry*, W. H. Freeman and Company, 5th ed., 2001.

[58] D. P. Tieleman, M. Sansom, and H. Berendsen, *Biophys. J.*, **76**(1), 40 (1999). Alamethicin Helices in a Bilayer and in Solution: Molecular Dynamics Simulations.

[59] J. F. Nagle and S. Trsitram-Nagle, *Curr. Opin. Struct. Biol.*, **10**(4), 474 (2000). Lipid Bilayer Structure.

[60] H. Scott, *Curr. Opin. Struct. Biol.*, **12**, 495 (2002). Modeling the Lipid Component of Membranes.

[61] U. Essmann and M. L. Berkowitz, *Biophys. J.*, **76**(4), 2081 (1999). Dynamical Properties of Phospholid Bilayers from Computer Simulations.

[62] E. Lindahl and O. Edholm, *Biophys. J.*, **79**(1), 426 (2000). Mesoscopic Undulations and Thickness Fluctuations in Lipid Bilayers from Molecular Dynamics Simulations.

[63] I. P. Sugar, T. E. Thompson, and R. L. Biltonen, *Biophys. J.*, **76**(4), 2099 (1999). Monte Carlo Simulations of Two-Component Bilayers: DMPC/DSPC Mixtures.

[64] A. Smondyrev and M. L. Berkowitz, *Biophys. J.*, **77**, 2075 (1999). Structure of Dipalmitoylphosphatidylcholine/Cholesterol Bilayer at Low and High Cholesterol Concentrations: Molecular Dynamics Simulations.

[65] S. W. Chiu, E. Jakobsson, and H. S. S. Subramaniam, *Biophys. J.*, **77**, 2462 (1999). Combined Monte Carlo and Molecular Dynamics Simulation of Fully Hydrated Dioleyl and Palmitoyl-Oleyl Phosphatidylcholine Lipid Bilayers.

[66] S. E. Feller, *Curr. Opin. Colloid Interface Sci.*, **5**, 217 (2000). Molecular Dynamics Simulations of Lipid Bilayers.

[67] E. Jakobsson, *Trends in Biochem. Sci.*, **22**, 339 (1997). Computer Simulation Studies of Biological Membranes: Progress, Promise and Pittfalls.

[68] G. Hummer, L. Pratt, and A. García, *J. Phys. Chem. A*, **102**(41), 7885 (1998). Molecular Theories and Simulation of Ions and Polar Molecules in Water.

[69] J. Bockris and A. Reddy, *Modern Electrochemistry*, Vol. I-Ionics, Plenum Press, New York, 2 ed., 1998.

[70] S. Li, M. Hoyles, S. Kuyucak, and S.-H. Chung, *Biophys. J.*, **74**(1), 37 (1998). Brownian Dynamics Study of Ion Transport in the Vestibule of Membrane Channels.

[71] J.-P. Simonin, L. Blum, and P. Turq, *J. Phys. Chem.*, **100**(18), 7704 (1996). Real Ionic Solutions in the Mean Spherical Approximation. 1. Simple Salts in the Primitive Model.

[72] J. Barthel, H. Krienke, and W. Kunz, *Physical Chemistry of Electrolyte Solutions*, number 5 in Topics in Physical Chemistry, Springer, New York, 1998.

[73] S. Durand-Vidal, J.-P. Simonin, and P. Turq, *Electrolytes at Interfaces*, Kluwer, 2000.

[74] W. Im, M. Feig, and C. Brooks III, *Biophys. J.*, **85**(5), 2900 (2003). An Implicit Membrane Generalized Born Theory for the Study of Structure, Stability, and Interactions of Membrane Proteins.

[75] D. P. Tieleman, L. R. Forrest, M. Sansom, and H. J. C. Berendsen, *Biochemistry*, **37**, 17554 (1998). Lipid Properties and the Orientation of Aromatic Residues in OmpF, Influenza M2, and Alamethicin Systems: Molecular Dynamics Systems.

[76] T. Schirmer and P. Phale, *J. Mol. Biol.*, **294**, 1159 (1999). Brownian Dynamics Simulation of Ion Flow Through Porin Channels.

[77] T. B. Wolf and B. Roux, *Protein: Struct., Funct. and Gen.*, **24**(1), 92 (1996). Structure, Energetics, and Dynamics of Lipid-Protein Interactions: A Molecular Dynamics Study of Gramicidin A Channel in a DMPC Bilayer.

[78] T. Lybrand, in *Reviews in Computational Chemistry*, K. B. Lipkowitz and D. B. Boyd, Eds., VHC Publishers, New York, 1990, Vol. 1, pp. 295–320. Computer Simulation of Biomolecular Systems Using Molecular Dynamics and Free Energy Perturbation Methods.

[79] D. P. Tieleman and H. J. C. Berendsen, *Biophys. J.*, **74**(6), 2786 (1998). A Molecular Dynamics Study of the Pores Formed by Escherichia coli OmpF Porin in a Fully Hydrated Palmitoyloleoylphosphatidylcholine Bilayer.

[80] L. Shen, D. Bassolino, and T. Souch, *Biochemistry*, **73**, 3 (1997). Transmembrane Helix Structure, Dynamics, and Interactions: Multi-Nanosecond Molecular Dynamics Simulations.

[81] P. Mezey, in *Reviews in Computational Chemistry*, K. B. Lipkowitz and D. B. Boyd, Eds., VHC Publishers, New York, 1990, Vol. 1, pp. 265–294. Molecular Surfaces.

[82] J. D. Faraldo-Gomez, G. R. Smith, and M. S. P. Sansom, *European Biophys. J.*, **31**, 217 (2002). Setting Up and Optimisation of Membrane Protein Simulations.

[83] R. Hockney and J. Eastwood, *Computer Simulation Using Particles*, Adam Hilger, Bristol, 1988.

[84] D. Levitt, *Biophys. J.*, **48**(1), 19 (1985). Strong Electrolyte Continuum Theory Solution for Equilibrium Profiles, Diffusion Limitation, and Conductance in Charged Ion Channels.

[85] M. Allen and D. Tildesley, *Computer Simulation of Liquids*, Clarendon Press, Oxford, 1987.

[86] Y. Georgalis, A. M. Kierzek, and W. Sa, *J. Phys. Chem. B*, **104**, 3405 (2000). Cluster Formation in Aqueous Electrolyte Solutions Observed by Dynamic Light Scattering.

[87] C. Jacoboni and P. Lugli, *The Monte Carlo Method for Semiconductor Device Equations*, Springer–Verlag, Wien, NewYork, 1989.

[88] P. Jordan, *Biophys. J.*, **39**(2), 157 (1982). Electrostatic Modeling of Ion Pores. I. Energy Barriers and Electric Field Profiles.

[89] P. Jordan, *Biophys. J.*, **41**(2), 189 (1983). Electrostatic Modeling of Ion Pores. II. Effects Attributable to the Membrane Dipole Potential.

[90] M. Cai and P. Jordan, *Biophys. J.*, **57**(4), 883 (1990). How Does Vestibule Surface Charge Affect Ion Conduction and Toxin Binding in a Sodium Channel?

[91] G. V. Miloshevsky and P. C. Jordan, *Biophys. J.*, **86**(2), 825 (2004). Anion Pathway and Potential Energy Profiles along Curvilinear Bacterial ClC Cl^- Pores: Electrostatic Effects of Charged Residues.

[92] W. Nonner, D. Chen, and B. Eisenberg, *Biophys. J.*, **74**(5), 2327 (1998). Anomalous Mole Fraction Effect, Electrostatics, and Binding in Ionic Channels.

[93] W. Nonner, L. Catacuzzeno, and B. Eisenberg, *Biophys. J.*, **79**(4), 1976 (2000). Binding and Selectivity in L-Type Calcium Channels: A Mean Spherical Approximation.

[94] D. Boda, D. Busath, D. Henderson, and S. Sokolowski, *J. Phys. Chem. B*, **104**(37), 8903 (2000). Monte Carlo Simulations of the Mechanism for Channel Selectivity: The Competition between Volume Exclusion and charge Neutrality.

[95] D. Boda, D. Gillespie, W. Nonner, D. Henderson, and B. Eisenberg, *Phys. Rev. E*, **68**, 046702 (2004). Computing Induced Charges in Inhomogeneous Dielectric Media: Application in a Monte Carlo Simulation of Complex Ionic Systems.

[96] D. Boda, D. Henderson, and D. Busath, *J. Phys. Chem. B*, **105**(47), 11574 (2001). Monte Carlo Study of the Effect of Ion and Channel Size on the Selectivity of a Model Calcium Channel.

[97] L. Greengard, *Science*, **265**(5174), 909 (1994). Fast Algorithms for Classical Physics.

[98] L. Greengard and V. Rokhlin, *J. Comput. Phys.*, **135**, 280 (1997). A Fast Algorithm for Particle Simulations.

[99] F. S. Lee and A. Warshel, *J. Chem. Phys.*, **97**(5), 3100 (1992). A Local Field Method for Fast Evaluation of Long-Range Electrostatic Interactions in Molecular Simulations.

[100] P. Ewald, *Ann. Phys.*, **64**, 253 (1921). Die Berechnung Optischer und Elektrostatischer Gitterpotentiale.

[101] M. Deserno and C. Holm, *J. Chem. Phys.*, **109**(18), 7678 (1998). How to Mesh Up Ewald Sums. I. A Theoretical and Numerical Comparison of Various Particle Mesh Routines.

[102] J. Jackson, *Classical Electrodynamics*, John Wiley & Sons, New York, 2^{nd} ed., 1975.

[103] H.-Q. Ding, N. Karasawa, and W. A. G. III, *J. Chem. Phys.*, **97**(6), 4309 (1992). Atomic Level Simulations on a Million Particles: The Cell Mulipole Method for Coulomb and London Nonbonded Interactions.

[104] J. Shimada, H. Kaneko, and T. Takada, *J. Comput. Chem.*, **15**(1), 29 (1994). Performance of Fast Mulipole Methods for Calculating Electrostatic Interactions in Biomacromolecular Simulations.

[105] C. A. White and M. Head-Gordon, *J. Chem. Phys.*, **101**(8), 6593 (1994). Derivation and Efficient Implementation of the Fast Mulitpole Method.

[106] T. Schlick, *Molecular Modeling and Simulation: An Interdisciplinary Guide*, Vol. 21 of *Interdisciplinary Applied Mathematics*, Springer, New York, 2000.

[107] A. W. Appel, *SIAM J. on Sci. Stat. Comput.*, **6**(1), 85 (1985). An Efficient Program for Many-Body Problems.

[108] E. L. Pollock and J. Glosli, *Comput. Phys. Commun.*, **95**, 93 (1996). Comments on P^3M, FMM, and the Ewald Method for Large Periodic Coulombic Systems.

[109] A. Leach, *Molecular Modelling Principles and Applications*, Prentice Hall, Harlow, England, 2^{nd} ed., 2001.

[110] P. Crozier, R. Rowley, D. Handerson, and D. Boda, *Chem. Phys. Lett.*, **325**(5-6), 675 (2000). A Corrected 3D Ewald Calculation of the Low Effective Temperature Properties of the Electrochemical Interface.

[111] D. M. Heyes, *J. Chem. Phys.*, **74**(3), 1924 (1981). Electrostatic Potentials and Fields in Infinite Point Charge Lattices.

[112] T. Darden, D. York, and L. Pedersen, *J. Chem. Phys.*, **98**(12), 10089 (1993). Particle Mesh Ewald: An Nlog(N) Method for Ewald Sums in Large Systems.

[113] A. Y. Toukmaji and J. A. Board, *Comp. Phys. Commun.*, **95**, 73 (1996). Ewald Summation Techniques in Perspective: A Survey.

[114] N. Karasawa and W. A. G. III, *J. Phys. Chem.*, **93**, 7320 (1989). Acceleration of Convergence for Lattice Sums.

[115] G. Rajagopal and R. J. Needs, *J. Comput. Phys.*, **115**, 399 (1994). An Optimized Ewald Method for Long-Ranged Potentials.

[116] U. Essmann, L. Perera, M. L. Berkowitz, T. Darden, H. Lee, and L. Pedersen, *J. Chem. Phys.*, **103**(19), 8577 (1995). A Smooth Particle Mesh Ewald Method.

[117] C. Pommerell and W. Fichtner, *SIAM J. on Sci. Stat. Comput.*, **15**(2), 460 (1994). Memory Aspects and Performance of Iterative Solvers.

[118] D. M. Young, *Iterative Solution of Large Linear Systems*, Computer Science and Applied Mathematics, Academic Press, New York, 1971.

[119] G. Dahlquist and Å. Björck, *Numerical Methods*, Prentice–Hall, Englewood Cliffs, N.J., 1974.

[120] P. J. Roache, *Computational Fluid Dynamics*, Hermosa Publishers, Albuquerque, N.M., 1976.

[121] B. Carré, *Computer Journal*, **4**(1), 73 (1961). The Determination of the Optimum Accelerating Factor for Successive Over–Relaxation.

[122] L. W. Ehrlich in M. H. Schultz, Eds., *Elliptic Problem Solvers*, pp. 255–259, New York, 1981. Academic Press.

[123] L. M. Adams and H. F. Jordan, *SIAM J. on Sci. Stat. Comput.*, **7**(2), 490 (1986). Is SOR Color–Blind ?

[124] S. Vandewalle, *Parallel Multigrid Waveform Relaxation for Parabolic Problems*, Teubner Skripten zur Numerik, B.G. Teubner, Stuttgart, Leipzig, 1993.

[125] W. Hackbush, *Multi-Grid Methods and Applications*, Springer–Verlag, Berlin, 1985.

[126] A. Brandt, *Mathematics of Computation*, **31**(138), 333 (1977). Multi-Level Adaptive Solutions to Boundary-Value Problems.

[127] A. Brandt in M. H. Schultz, Eds., *Elliptic Problem Solvers*, pp. 39–84, New York, 1981. Academic Press.

[128] P. S. Ramanathan and H. L. Friedman, *J. Chem. Phys.*, **54**(3), 1086 (1971). Study of a Refined Model for Aqueous 1-1 Electrolytes.

[129] R. Berry, S. Rice, and J. Ross, *Physical Chemistry*, Oxford University Press, 2^{nd} ed., 2000.

[130] W. Im, S. Seefeld, and B. Roux, *Biophys. J.*, **79**(2), 788 (2000). A Grand Canonical Monte Carlo-Brownian Dynamics Algorithm for Simulating Ion Channels.

[131] M. Wilson, A. Pohrille, and L. Pratt, *J. Chem. Phys.*, **83**(11), 5832 (1985). Molecular Dynamic Test of the Brownian Description of Na^+ Motion in Water.

[132] Y. Yang, D. Henderson, P. Crozier, R. Rowley, and D. Busath, *Mol. Phys.*, **100**(18), 3011 (2001). Permeation of Ions Through a Model Biological Channel: Effect of Periodic Boundary Conditions and Cell Size.

[133] B. Nadler, T. Naeh, and A. Schuss, *SIAM J. Appl. Math.*, **63**(3), 850 (2003). Connecting a Discrete Ionic Simulation to a Continuum.

[134] B. Corry, M. Hoyles, T. Allen, M. Walker, S. Kuyucak, and S.-H. Chung, *Biophys. J.*, **82**(4), 1975 (2002). Reservoir Boundaries in Brownian Dynamics Simulations of Ion Channels.

[135] C. Birdsall and A. Langdon, *Plasma Physics via Computer Simulation*, Institute of Physics Publishing, Bristol and Philadelphia, 1991.

[136] R. Eisenberg, *J. Membr. Biol.*, **150**(1), 1 (1996). Computing the Field in Proteins and Channels.

[137] A. Syganow and E. von Kitzing, *Biophys. J.*, **76**(2), 768 (1999). (In)validity of the Constant Field and Constant Currents Assumptions in Theories of Ion Transport.

[138] B. Roux and S. Bernèche, *Biophys. J.*, **82**(3), 1681 (2002). On the Potential Functions used in Molecular Dynamics Simulations of Ion Channels.

[139] D. Ermak, *J. Chem. Phys.*, **62**(10), 4189 (1975). A Computer Simulation of Charged Particles in Solution. I. Technique and Equilibrium Properties.

[140] P. Turq, F. Lantelme, and H. Friedman, *J. Chem. Phys.*, **66**(7), 3039 (1977). Brownian Dynamics: Its Application to Ionic Solutions.

[141] W. van Gunsteren and H. Berendsen, *Mol. Phys.*, **45**(3), 637 (1982). Algorithms for Brownian Dynamics.

[142] L. Verlet, *Phys. Rev.*, **159**(1), 159 (1967). Computer "Experiments" on Classical Fluids. I. Thermodynamical Properties of Lennard-Jones Molecules.

[143] E. Jakobsson, *Method. Enzymol.*, **14**, 342 (1998). Using Theory and Simulation to Understand Permeation and Selectivity in Ion Channels.

[144] P. Crozier, D. Henderson, R. Rowley, and D. Busath, *Biophys. J.*, **81**(6), 3077 (2001). Model Channel Ion Currents in NaCl-Extended Simple Point Charge Water Solution with Applied-Field Molecular Dynamics.

[145] P. Crozier, R. Rowley, N. B. Holladay, D. Henderson, and D. D. Busath, *Phys. Rev. Lett.*, **86**(11), 2467 (2001). Molecular Dynamics Simulation of Continuous Current Flow Through a Model Biological Membrane Channel.

[146] W. Jorgensen, J. Chandrasekhar, J. Madura, R. Impey, and M. Klein, *J. Chem. Phys.*, **79**(2), 926 (1983). Comparison of Simple Potential Functions for Simulating Liquid Water.

[147] A. Wallqvist and R. Mountain, in *Reviews in Computational Chemistry*, K. B. Lipkowitz and D. B. Boyd, Eds., VHC Publishers, New York, 1999, Vol. 13, pp. 183–247. Molecular Models of Water: Derivation and Description.

[148] H. Berendsen, J. Postma, W. van Gunsteren, and J. Hermans in *Intermolecular Forces*, B. Pullman, Ed.; Reidel, Dodrecht, Holland, 1981; pp. 331–342.

[149] W. Jorgensen, *J. Chem. Phys.*, **77**(7), 4156 (1982). Revised TIPS for Simulation of Liquid Water and Aqueous Solutions.

[150] H. Berendsen, J. Grigera, and T. Straatsma, *J. Phys. Chem.*, **91**, 6269 (1987). The Missing Term in Effective Pair Potentials.

[151] T. Schlick in P. Deuflhard, J. Hermans, B. Leimkuhler, A. Mark, S. Reich, and R. Skeel, Eds., *Computational Molecular Dynamics: Challenges, Methods, Ideas*, Vol. 4 of *Lecture Notes in Computational Science and Engineering*, pp. 227–262, New York, 1997. Springer.

[152] M. Tuckerman, B. J. Berne, and G. J. Martyna, *J. Chem. Phys.*, **97**(3), 1990 (1992). Reversible Multiple Time Scale Molecular Dynamics.

[153] X. Qian and T. Schlick, *J. Chem. Phys.*, **116**(14), 5971 (2002). Efficient Multiple-Time-Step Integrators with Distance-Based Force Splitting for Particle-Mesh-Ewald Molecular Dynamics Simulations.

[154] T. Schlick, *Molecular Modeling and Simulation*, Vol. 21 of *Interdisciplinary Appplied Mathematics*, Springer, New York, 2002.

[155] S. Bernèche and B. Roux, *Biophys. J.*, **78**(6), 2900 (2000). Molecular Dynamics of the KcsA K^+ Channel in a Bilayer Membrane.

[156] S. Bernèche and B. Roux, *Nature*, **414**, 73 (2001). Energetics of Ion Conduction Through the K^+ Channel.

[157] T. Straatsma, in *Reviews in Computational Chemistry*, K. B. Lipkowitz and D. B. Boyd, Eds., VHC Publishers, New York, 1996; Vol. 9, pp. 81–127. Free Energy by Molecular Simulation.

[158] S. Bernèche and B. Roux, *PNAS*, **100**(15), 8644 (2003). A Microscopic View of Ion Conduction Through the K^+ Channel.

[159] S. Chiu, J. Novotny, and E. Jakobsson, *Biophys. J.*, **64**(1), 98 (1993). The Nature of Ion and Water Barrier Crossings in a Simulated Ion Channel.

[160] A. B. Mamonov, R. D. Coalson, A. Nitzan, and M. G. Kurnikova, *Biophys. J.*, **84**(6), 3646 (2003). The Role of the Dielectric Barrier in Narrow Biological Channels: A Novel Composite Approach to Modeling Single-Channel Currents.

[161] B. Roux, *Biophys. J.*, **77**(1), 139 (1999). Statistical Mechanical Equilibrium Theory of Selective Ion Channels.

[162] G. Torrie and J. Valleau, *J. Comput. Phys.*, **23**, 187 (1977). Nonphysical sampling distributions in Monte Carlo free-energy estimation: Umbrella sampling.

[163] O. Becker, A. MacKerell, B. Roux, and M. Watanabe, Eds., *Computational Biochemistry and Biophysics*, Marcel Dekker, Inc., New York, Basel, 2001.

[164] D. Beglov and B. Roux, *J. Chem. Phys.*, **100**(12), 9050 (1994). Finite Representations of an Infinite Bulk System: Solvent Boundary Potential for Computer Simulations.

[165] M. Jalaie, in *Reviews in Computational Chemistry*, K. B. Lipkowitz and D. B. Boyd, Eds., VHC Publishers, New York, 2000, Vol. 14, pp. 441–486.

Published Force Field Parameters for Molecular Mechanics, Molecular Dynamics, and Monte Carlo Simulations

[166] T. Halgren and W. Damm, *Curr. Opin. Struct. Biol.*, **11**(2), 236 (2001). Polarizable Force Fields.

[167] S. Rick and S. Stuart, in *Reviews in Computational Chemistry*, K. B. Lipkowitz and D. B. Boyd, Eds., VHC Publishers, New York, 2002, Vol. 18, pp. 89–146. Potentials and Algorithms for Incorporating Polarizability in Computer Simulations.

[168] T. Allen, S. Kuyucak, and S.-H. Chung, *J. Chem. Phys.*, **111**(17), 7985 (1999). The Effect of Hydrophobic and Hydrophilic Channel Walls on the Structure and Diffusion of Water and Ions.

[169] C. Domene and M. S. P. Sansom, *Biophys. J.*, **85**(5), 2787 (2003). Potassium Channel, Ions, and Water: Simulation Studies Based on the High Resolution X-Ray Structure of KcsA.

[170] S. Rick, S. Stuart, and B. Berne, *J. Chem. Phys.*, **101**(7), 6141 (1994). Dynamical Fluctuating Charge Force Fields: Application to Liquid Water.

[171] J. Banks, G. Kaminsky, R. Zhou, D. Mainz, B. Berne, and R. Friesner, *J. Chem. Phys.*, **110**(2), 741 (1999). Parametrizing a Polarizable Force Field from *Ab Initio* Data. I. The Fluctuating Point Charge Model.

[172] H. Stern, G. Kaminski, J. Banks, R. Zhou, B. Berne, and R. Friesner, *J. Phys. Chem. B*, **103**(22), 4730 (1999). Fluctuating Charge, Polarizable

Dipole, and Combined Models: Parametrization from *Ab Initio* Quantum Chemistry.

[173] B. Arbuckle and P. Clancy, *J. Chem. Phys.*, **116**(12), 5090 (2002). Effects of the Ewald Sum on the Free Energy of the Extended Simple Point Charge Model for Water.

[174] J. Hermans, H. Berendsen, W. van Gunsteren, and J. Postma, *Biopolymers*, **23**, 1513 (1984). A Consistent Empirical Potential for Water-Protein Interactions.

[175] H. Alper and R. Levy, *J. Chem. Phys.*, **91**(2), 1242 (1989). Computer Simulation of the Dielectric Properties of Water: Studies of the Simple Point Charge and Transferrable Intermolecular Potential Models.

[176] S. Chiu, E. Jakobsson, S. Subramaniam, and J. McCammon, *Biophys. J.*, **60**(1), 273 (1991). Time-Correlation Analysis of Simulated Water Motion in Flexible and Rigid Gramicidin Channels.

[177] A. Fick, *Annalen der Physik und Chemie*, **94**, 59 (1855). Über Diffusion.

[178] C. Gardiner, *Handbook of Stochastic Methods for Physics, Chemistry and the Natural Sciences*, number 13 in Springer Series in Synergetics, Springer, New York, 1983.

[179] P. E. Kloeden and E. Platen, *Numerical Solution of Stochastic Differential Equations*, number 23 in Applications of Mathematics, Springer-Verlag, corrected 3^{rd} ed., 1999.

[180] R. Eisenberg, M. Klosek, and Z. Schuss, *J. Chem. Phys.*, **102**(4), 1767 (1995). Diffusion as a Chemical Reaction: Stochastic Trajectories Between Fixed Concentrations.

[181] D. McQuarrie, *Statistical Mechanics*, University Science Books, Sausalito, CA, 2000.

[182] S. Rice and P. Gray, *The Statistical Mechanics of Simple Liquids*, Vol. 8 of *Monographs in Statistical Physics and Thermodynamics*, Wiley Interscience, New York, 1965.

[183] N. W. Ashcroft and N. Mermin, *Solid State Physics*, Holt–Sauders International Editions, Tokyo, 1981.

[184] G. Baccarani and M. Wordeman, *Solid-State Electron.*, **28**, 407 (1985). An Investigation of Steady State Velocity Overshoot Effects in Si and GaAs Devices.

[185] D. Chen, R. Eisenberg, J. Jerome, and C. Shu, *Biophys. J.*, **69**, 2304 (1995). Hydrodynamic Model of Temperature Change in Open Ionic Channels.

[186] C. M. Snowden, *Introduction to Semiconductor Device Modelling*, World Scientific Publishing, Singapore, 1986.

[187] H. Gummel, *IEEE Trans. Elect. Dev.*, **ED-11**, 455 (1964). A Self-Consistent Iterative Scheme for One-Dimensional Steady State Transistor Calculations.

[188] D. Sharfetter and H. Gummel, *IEEE Trans. Elect. Dev.*, **ED-16**(1), 64 (1969). Large-Signal Analysis of a Silicon Read Diode Oscillator.

[189] J. Molenaar Multigrid Methods for Semiconductor Device Simulation Technical Report CWI TRACT 100, Center for Mathematics and Computer Science, P.O. Box 4079, 1090 GB Amsterdam, The Netherlands, (1993).

[190] D. Levitt, *Biophys. J.*, **52**(3), 455 (1987). Exact Continuum Solution for a Channel that Can be Occupied by Two Ions.

[191] A. E. Cardenas, R. D. Coalson, and M. G. Kurnikova, *Biophys. J.*, **79**(1), 80 (2000). Three-Dimensional Poisson-Nernst-Planck Theory Studies: Influence of Membrane Electrostatics on Gramicidin A Channel Conductance.

[192] T. van der Straaten, S. Varma, S. Chiu, J. Tang, N. Aluru, R. Eisenberg, U. Ravaioli, and E. Jakobsson in M. Laudon and B. Romanowicz, Eds., *Proceedings of the Second International Conference on Computational Nanoscience and Nanotechnology - ICCN2002*, pp. 60–63, San Juan, PR, 2002. Computational Publications, MA.

[193] R. Eisenberg, *J. Membr. Biol.*, **150**, 1 (1996). Computing the Field in Protein and Channels.

[194] B. Honig and A. Nichols, *Science*, **268**, 1144 (1995). Classical Electrostatics in Biology and Chemistry.

[195] G. Lamm, in *Reviews in Computational Chemistry*, K. B. Lipkowitz and D. B. Boyd, Eds., VHC Publishers, New York, 2003, Vol. 19, pp. 147-365. The Poisson-Boltzmann Equation.

[196] T. Weiss, *Cellular Biophysics*, Vol. 1-2, MIT Press, Cambridge, MA, 1966.

[197] B. Corry, S. Kuyucak, and S.-H. Chung, *J. Gen. Physiol.*, **114**, 597 (1999). Test of Poisson-Nernst-Plank Theory in Ion Channels.

[198] B. Corry, S. Kuyucak, and S.-H. Chung, *Biophys. J.*, **78**(5), 2364 (2000). Tests of Continuum Theories as Models of Ion Channels. II. Poisson-Nernst-Planck Theory versus Brownian Dynamics.

[199] G. Moy, B. Corry, S. Kuyucak, and S.-H. Chung, *Biophys. J.*, **78**(5), 2349 (2000). Tests of Continuum Theories as Models of Ion Channels. I. Poisson-Boltzmann Theory versus Brownian Dynamics.

[200] B. Nadler, U. Hollerbach, and R. Eisenberg, *Phys. Rev. E*, **68**, 021905 (2003). Dielectric Boundary Force and Its Crucial Role in Gramicidin.

[201] B. Corry, S. Kuyucak, and S.-H. Chung, *Biophys. J.*, **84**(6), 3594 (2003). Dielectric Self-Energy in Poisson-Boltzmann and Poisson-Nernst-Planck Models of Ion Channels.

[202] R. S. Eisenberg in *Proceedings of the Biophysical Society Meeting*. Biophysical Society, 1993. From Structure to Permeation in Open Ionic Channels.

[203] R. S. Eisenberg, in *New Developments and Theoretical Studies of Proteins*, World Scientific, London, 1996; Vol. 7 of *Advanced Series in Physical*

Chemistry; chapter 7, pp. 269–358; Atomic Biology, Electrostatics, and Ionic Channels.

[204] R. Mashl, Y. Tang, J. Schnitzer, and E. Jakobsson, *Biophys. J.*, **81**(5), 2473 (2001). Hierarchical Approach to Predicting Permeation in Ion Channels.

[205] M. F. Schumaker, R. Pomes, and B. Roux, *Biophys. J.*, **79**(6), 2840 (2000). A Combined Molecular Dynamics and Diffusion Model of Single Proton Conduction through Gramicidin.